# nature methods



# De novo construction of T cell compartment in humanized mice engrafted with iPSC-derived thymus organoids

Ann Zeleniak 1, Connor Wiegand 2,8, Wen Liu<sup>1,8</sup>, Catherine McCormick 3,8, Ravikumar K.<sup>2</sup>, Amir Alavi 4, Haonan Guan<sup>3</sup>, Suzanne Bertera 1, Robert Lakomy Asako Tajima Henry Cohen Stephanie Wong Lame Balikani 5, Benjamin Mizerak<sup>2</sup>, Ziv Bar-Joseph Massimo Trucco 1,3,6, Ipsita Banerjee<sup>2</sup> and Yong Fan 1,3,6,7 \infty

Hematopoietic humanized (hu) mice are powerful tools for modeling the action of human immune system and are widely used for preclinical studies and drug discovery. However, generating a functional human T cell compartment in hu mice remains challenging, primarily due to the species-related differences between human and mouse thymus. While engrafting human fetal thymic tissues can support robust T cell development in hu mice, tissue scarcity and ethical concerns limit their wide use. Here, we describe the tissue engineering of human thymus organoids from inducible pluripotent stem cells (iPSC-thymus) that can support the de novo generation of a diverse population of functional human T cells. T cells of iPSC-thymus-engrafted hu mice could mediate both cellular and humoral immune responses, including mounting robust proinflammatory responses on T cell receptor engagement, inhibiting allogeneic tumor graft growth and facilitating efficient Ig class switching. Our findings indicate that hu mice engrafted with iPSC-thymus can serve as a new animal model to study human T cell-mediated immunity and accelerate the translation of findings from animal studies into the clinic.

hile animal models have contributed substantially to our understanding of human physiology and disease, one of the main hurdles in translating these findings into the clinic is the existence of species-specific differences between humans and animals1. Humanized (hu) mice, in which human cells of hematopoietic lineage are transplanted into NOD. scid.IL2rgnull (NSG) or other immunodeficient IL2rgnull mouse lines, are powerful models that are used broadly to overcome these challenges<sup>2-4</sup>. Based on the types of hematopoietic cell infused and the methods used for human cell engraftment, hu mice can be grouped into three main categories: the hu.PBMC model, which is transplanted with mature peripheral blood mononuclear cells (PBMCs); the hu.SRC (scid-repopulating cell) model, which is infused with CD34<sup>+</sup> hematopoietic stem cells (HSCs) that can produce cells of all the hematopoietic lineages and the hu.BLT (bone marrow, liver and thymus) model, in which pieces of human fetal thymus and liver are cotransplanted underneath the kidney capsules of immunodeficient IL2rgmull recipients, followed by intravenous infusion of CD34+ HSCs from the same fetal donor<sup>5,6</sup>.

Each of these hu models has advantages and disadvantages in modeling human immune responses. For example, while the function of both mature human lymphoid and myeloid cells can be readily assessed in hu.PBMC mice, they develop lethal, xenogeneic graft-versus-host disease (GVHD) within weeks after transplantation, preventing their use for long-term studies<sup>3</sup>. In contrast,

long-term engraftment of all hematopoietic lineage cells can be achieved in hu.SRC mice. However, human T cells are educated and restricted by murine major histocompatibility complexes (MHCs) within the endogenous mouse thymus, which limit their function in mediating adaptive immune response. Engrafted fetal thymic tissues can successfully support the production of functional human T cells in hu.BLT mice, which have been instrumental in studying HIV and other infectious diseases. Yet, ethical concerns associated with the use of human fetal tissues and their scarcity limit their widespread usage.

The thymus gland does not contain HSCs capable of self-renewal, relying instead on the continuous recruitment of thymus settling/ seeding progenitors (TSPs) coming from the bone marrow to maintain long-term thymopoiesis<sup>8</sup>. Once inside the thymus, TSPs undergo a series of differentiation events, including T-lineage specification and positive and negative selection, to become mature T cells<sup>9-11</sup>. Thymic epithelial cells (TECs), the predominant population of cells in the thymus stroma, play essential regulatory roles throughout thymopoiesis<sup>12</sup>. TECs within the cortical region (cTECs) provide key signals for T cell fate specification and positively select T cells that can functionally interact with the body's own antigen present cells (APCs)<sup>13-15</sup>. Conversely, TECs within the medullary region (mTECs) possess the unique characteristic of expressing and presenting tissue specific self-antigens (TSAs)<sup>16</sup>. The mTECs are critical for eliminating T cells with high auto-reactivity in the

'Institute of Cellular Therapeutics, Allegheny Health Network, Pittsburgh, PA, USA. <sup>2</sup>Department of Chemical and Petroleum Engineering, University of Pittsburgh, PH, USA. <sup>3</sup>Department of Biological Sciences, Carnegie Mellon University, Pittsburgh, PA, USA. <sup>4</sup>Department of Computational Biology, Carnegie Mellon University, Pittsburgh, PA, USA. <sup>5</sup>Department of Pathology and Laboratory Medicine, Allegheny General Hospital, Pittsburgh, PA, USA. <sup>6</sup>Department of Microbiology and Immunology, Drexel University College of Medicine, Philadelphia, PA, USA. <sup>7</sup>Department of Biomedical Engineering, Carnegie Mellon University, Pittsburgh, PA, USA. <sup>8</sup>These authors contributed equally: Connor Wiegand, Wen Liu, Catherine McCormick. <sup>™</sup>e-mail: yong.fan@ahn.org

thymus, supporting the development of regulatory T cells and thus maintaining immunologic self-tolerance<sup>17</sup>.

We, and others, have shown that functional thymus organoids can be constructed by repopulating decellularized thymus scaffolds with isolated murine TECs<sup>18,19</sup>. The three-dimensional (3D) network of extracellular matrix in the decellularized thymus scaffolds can maintain the long-term survival and function of TECs both in vitro and in vivo. When transplanted under the kidney capsule of athymic nude mice, tissue-engineered murine thymus organoids can support the generation of a diverse and functional repertoire of T cells in the recipient mice<sup>20</sup>. Recently, Campinoti and colleagues have shown that functional human thymus can be reconstituted by seeding rat thymus scaffolds with in vitro expanded thymic stromal progenitors isolated from postnatal donors, highlighting the feasibility of the tissue-engineering approach in thymus regeneration<sup>21</sup>.

Induced pluripotent stem cells (iPSCs) have been widely used in regenerative medicine, and have been proposed as a renewable source of TECs for thymus tissue engineering<sup>22</sup>. Since the seminal concurrent reporting from Parent et al.<sup>23</sup> and Sun et al.<sup>24</sup>, great progresses have been made in generating TEC progenitor cells (TEPCs) from human pluripotent stem cells (hPSCs, both embryonic and induced)<sup>25–27</sup>. When transplanted underneath the kidney capsules of athymic nude mice, TEPCs, either derived from human embryonic stem cells (hESCs) or iPSCs, have been shown to mature into functional TECs and support the development of polyclonal murine T cells. Here, we describe the generation of functional human thymus organoids from iPSCs that can support the development of human T cells from CD34+ hematopoietic progenitor cells (HPCs) in hu mice.

#### Results

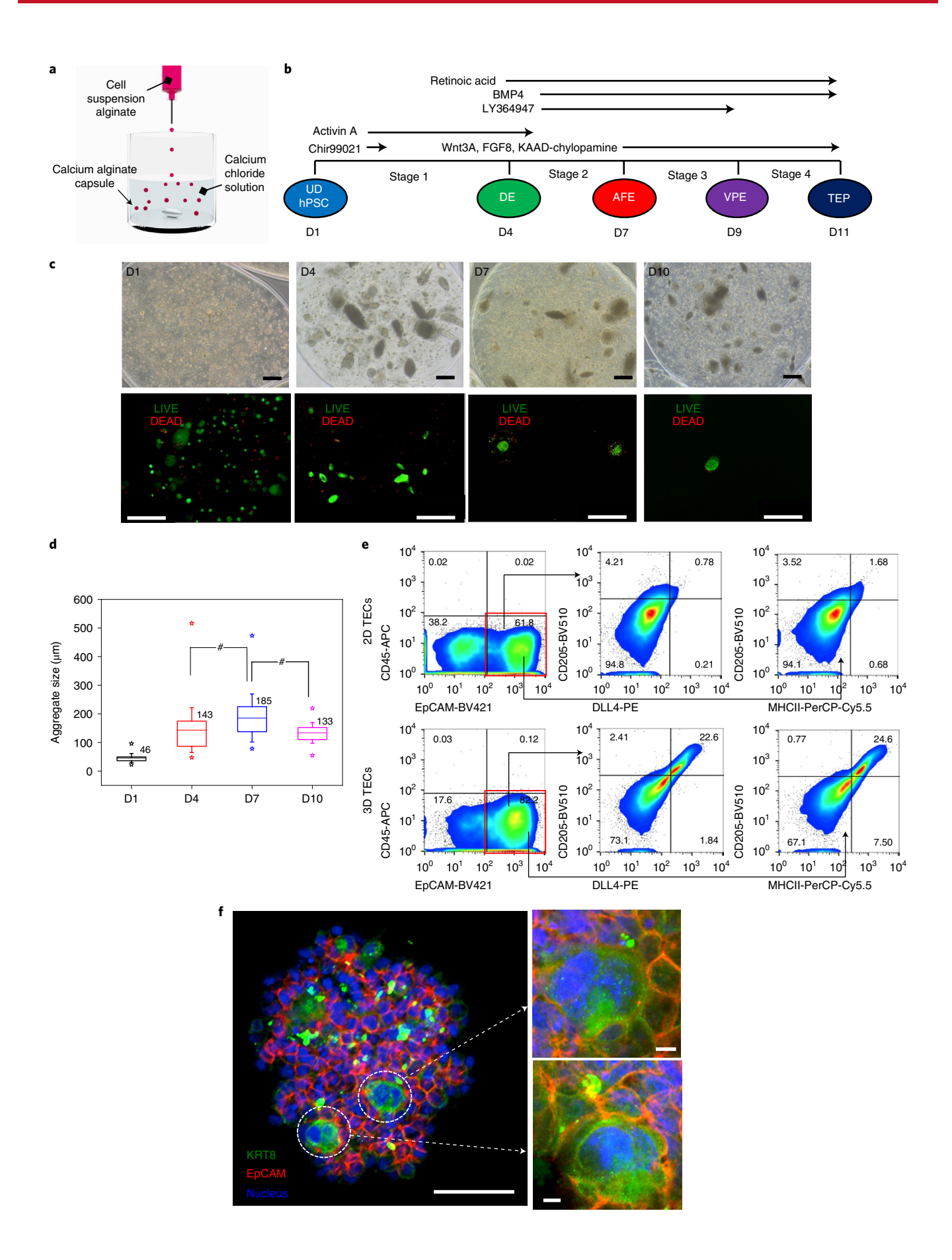
Differentiation of iPSCs into TEPCs in 3D alginate capsules. We have previously shown that encapsulation of hESCs within 3D alginate capsules not only facilitates their propagation when maintained at the pluripotent state, but also enhances their differentiation into pancreatic islet-like cells on induction, as compared to 2D culture<sup>28</sup>. A similar approach was adopted to promote the differentiation of human iPSCs into TEPCs with a modified four-stage induction protocol<sup>23,24,28</sup> (Fig. 1a,b). Single iPSCs encapsulated in alginate proliferated at undifferentiated stage into small aggregates of approximately 50 µm in diameter after 4 to 6 days of culture (Fig. 1c,d). Initial induction toward definitive endoderm (between days 1-4, D1-D4) resulted in increased mean aggregate sizes (box plot, Fig. 1d) and a shift in the distribution toward larger aggregate sizes (Supplementary Fig. 1a). The average size of aggregates peaked at D7, and decreased slightly on induction of further differentiation toward TEPC lineage at D10 (Fig. 1d). Similar patterns of TEPC aggregate formation were observed in differentiating hESCs (Supplementary Fig. 1b-d).

The overall efficiency of iPSC to TEPC differentiation was evaluated by examining the surface expression of EpCAM, a key TEC marker, with flow cytometry (FCM). About  $84.6\pm13\%$  (n=5) of iPSC-derived TEPCs were EpCAM+ (Fig. 1e). Notably, a substantial population of EpCAM+ cells was CD205+DLL4+MHCII+, suggesting that the 3D platform can facilitate the maturation of TEPCs into cTEC subsets (Fig. 1e, right panels). In corroboration with the FCM data, immunofluorescence analyses showed the presence of both CD205+ and DLL4+ cells (Supplementary Fig. 2). In addition, a unique group of EpCAM+ cells coexpressing high levels of *KRT8*, the cytokeratin gene expressed in both TEC progenitors and cTECs (Fig. 1f), was observed. These data highlight the successful progression of iPSC differentiation into TEC subsets.

To further characterize the iPSC-TECs, we analyzed the expression of TEC-specific markers by bulk quantitative PCR with reverse transcription (RT-qPCR) (Extended Data Fig. 1). In line with previous reports, increased expression of ventral pharyngeal endoderm (VPE), TEPC markers (EYA1 and FOXN1), loss of stem cell (OCT4 and SOX2) and definitive endoderm (SOX17) markers were observed, suggesting successful induction of TEPC lineage specification (Extended Data Fig. 1c,d). Marked increases in expression of cytokeratin genes (for example, sixfold for KRT17, fivefold for KRT18) were seen in TEPCs generated in the 3D alginate capsules when compared to those derived from the 2D culture, suggesting their epithelial nature (Extended Data Fig. 1a). Moreover, cTEC-specific genes critical for self-antigen processing and positive selection functions (for example, PRSS16, ACKR4 and PSMB11) were expressed at significantly higher levels in 3D TECs (Extended Data Fig. 1b). DLL4, one of the Notch ligands present on the surface of cTECs that is essential for T-lineage specification is also elevated (Extended Data Fig. 1b). Similarly, the expression of AIRE, a key transcriptional regulator for TSA expression in mTECs, was promoted solely in the 3D culture. Consistently, a similar expression pattern was shared by CSN2, a TSA whose expression in mTECs is regulated by AIRE (Extended Data Fig. 1e). Such TEC-specific gene expression patterns were also detected in hESC differentiation into TEPCs (Supplementary Fig. 3), but not observed in iPSC-derived islet aggregates generated from the same 3D platform with islet cell differentiation protocol (Supplementary Fig. 4), suggesting further the specificity of our protocol to induce TEC differentiation.

FOXN1 is a master regulator for TEC lineage specification during thymus organogenesis and is critical for maintaining TEC function in postnatal thymus<sup>29,30</sup>. To further evaluate the expression of FOXN1 in 3D iPSC-TECs, we performed immunofluorescence analysis, using in vitro propagated human primary TECs (passage 02 post isolation, P2 hTECs) and lymph node fibroblastic cells as positive and negative controls, respectively. As shown in Extended Data Fig. 2, FOXN1 expression was readily detectable in iPSC-TECs, but not in fibroblastic controls. Of note, only a subset of primary P2 hTECs displayed strong FOXN1 staining, presumably due to their

**Fig. 1 | Differentiation of human iPSCs into TEPCs in 3D alginate hydrogel capsule. a**, Schematic illustration of iPSC embedding and differentiation in 3D alginate capsule. **b**, Differentiation timeline of iPSCs into TEPCs. UD, undifferentiated; DE, definitive endoderm; AFE, anterior foregut endoderm; TEP, thymic epithelial progenitor. **c**, Images of iPSC aggregates at different stages of TEPC differentiation. Top panels, bright field photographic images of iPSC aggregates within the alginate capsules at days 1, 4, 7 and 10 (D1-D10) after initiation of differentiation; blue scale bar, 200 μm. Lower panels, survival of iPSC-derived TEPC aggregates in alginate capsules. Green, live cells with calcein-AM staining; red, dead cells stained with ethidium homodimer-1. Shown are representative images from three independent iPSC-TEC differentiation batches with similar results. Upper scale bars, 200 μm; lower scale bars, 500 μm. **d**, Size distribution of iPSC aggregates at different stages of TEPC differentiation. The boxes indicate the interquartile range (25-75th percentile) and the whiskers indicate the standard deviation of the distribution. The mean is denoted by the line across the box and the maximum and minimum is denoted by the 'star' symbol. '#' indicates statistically significant distribution as determined by one way analysis of variance and post hoc Tukey test with a *P* = 0.05. All groups are statistically significant with respect to D1. **e**, Representative FCM analysis of surface expression of TEC lineage markers in 2D- and 3D-cultured iPSC-TECs. All markers were analyzed within the CD45-EpCAM<sup>+</sup> gate (red boxes in the left columns). **f**, Immunofluorescent images of 3D iPSC-TEC aggregates stained with antibodies against EpCAM (red) and cytokeratin-8 (KRT8, green). White scale bar, 50 μm. Right-hand inserts, high magnification images of the indicated areas; white scale bars, both 5 μm. Shown are representative images from three independent iPSC-TEC differentiations with similar results.



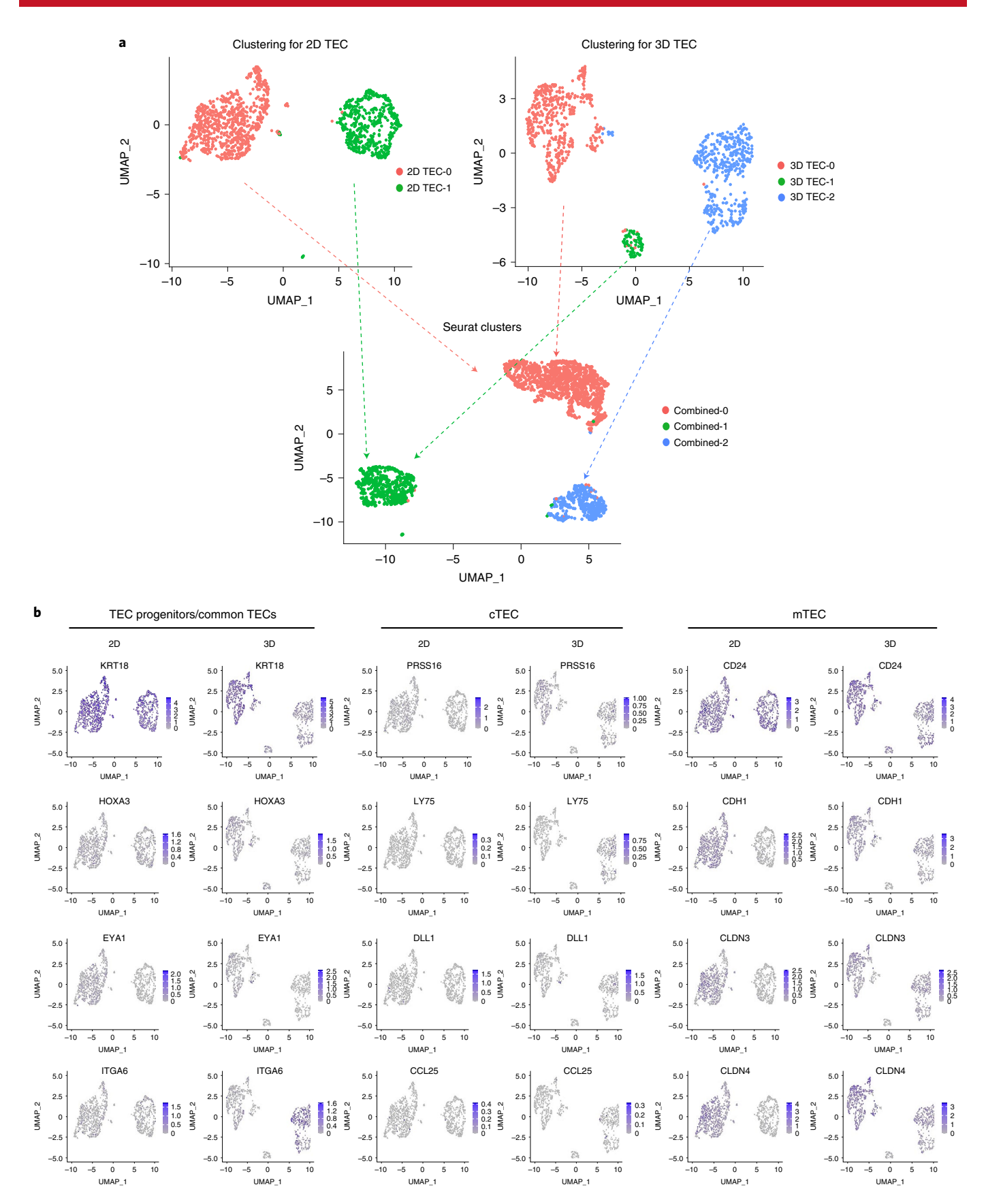


**Fig. 2** | scRNA-seq analysis of iPSC-TECs. a, UMAP visualization of 2D and 3D iPSC-TEC datasets. The UMAP graph in the bottom panel represents the clusters of the combined datasets, with the corresponding 2D and 3D clusters connected by the arrows. b, Annotation of expression of representative TEC progenitor/common TEC (*KRT8/KRT18, HOXA3, EYA1* and *ITGA6*), cTEC (*PRSS16, LY75, DLL1* and *CCL25*) and mTEC (*CD24, CDH1, CLDN3* and *CLDN4*) specific genes in 2D and 3D clusters. The intensity of purple indicates the levels of gene expression.

exposure to 2D culture in vitro, as it has been shown that TECs cultured under 2D conditions rapidly lose their TEC-specific molecular signature and function (Extended Data Fig. 2 and Supplementary Fig. 5)<sup>31</sup>. Indeed, lower levels of FOXN1 transcripts were detected in primary P2 hTECs when compared with freshly isolated human thymus, further suggesting the importance of maintaining 3D configuration for TEC differentiation and culture (Supplementary Fig. 6). Nevertheless, while much higher than those of 2D iPSC-TECs, FOXN1 expression in 3D iPSC-TECs remained much lower than human thymus, highlighting the need for further protocol optimization to generate mature and functional TECs from human iPSCs (Extended Data Fig. 1d and Supplementary Fig. 6).

Phenotypic characterization of iPSC-TECs with single-cell RNA-sequencing (scRNA-seq). Expression of markers of non-TEC lineage cells, such as VPE-derived parathyroid epithelial primordium marker GCM2, and mesenchymal/fibroblastic marker PDGFRA, was also detected in 2D and 3D iPSC-TECs by RT-qPCR, suggesting that the iPSC-TECs might not represent a uniformed differentiated product, but rather heterogeneous populations under these conditions (Extended Data Fig. 1f). To further characterize the iPSC-TEC populations generated by either 2D or 3D differentiation, scRNA-seq analysis was carried out to profile the transcriptome of individual cells and their relevance to TEC subsets of human thymus was projected. Unsupervised cell clustering analysis showed two and three major cell clusters in the 2D (2D TEC-0 and -1) and 3D (3D TEC-0, -1 and -2) iPSC-TECs, respectively (Fig. 2a). To facilitate the annotation of the iPSC-TEC clusters, we first examined the expression pattern of marker genes specific for published TEC subtypes<sup>21,32</sup>, including common TECs and TEC progenitors (ITGA6, HOX3, EYA1, KRT18), cTECs (PSMB11, LY75, PRSS16, CD274) and mTECs (CD24, CDH1, CLDN3 and CLDN4), as well as markers that are associated with other TEC properties, such as the antigen presenting function (CD74, HLA-DPB1, HLA-DQB1, HLA-DRB1) (Fig. 2b and Extended Data Fig. 3a). Consistent with the bulk RT-qPCR results, TEC epithelial markers showed increased expression in 3D iPSC-TEC clusters when compared to 2D clusters.

To investigate the correlation between the 2D and 3D iPSC-TECs, the two datasets were aligned and the cells were grouped into three combined clusters (0–2) on the same uniform manifold approximation and projection (UMAP) plot (Fig. 2a). The resulting integration of the two datasets suggests that iPSCs followed similar TEC specification/differentiation programs under both the 2D and 3D conditions. Combined cluster 0 represented the largest populations of both 2D and 3D iPSC-TECs (2D TEC-0 and 3D TEC-0, respectively), with a predominant transcriptional signature of epithelial cells, especially those associated with mTECs and progenitors (Fig. 2b)<sup>33</sup>. In contrast, cells in combined cluster 1 (corresponding to 2D TEC-1 and 3D TEC-2) express both epithelial and mesenchymal markers,

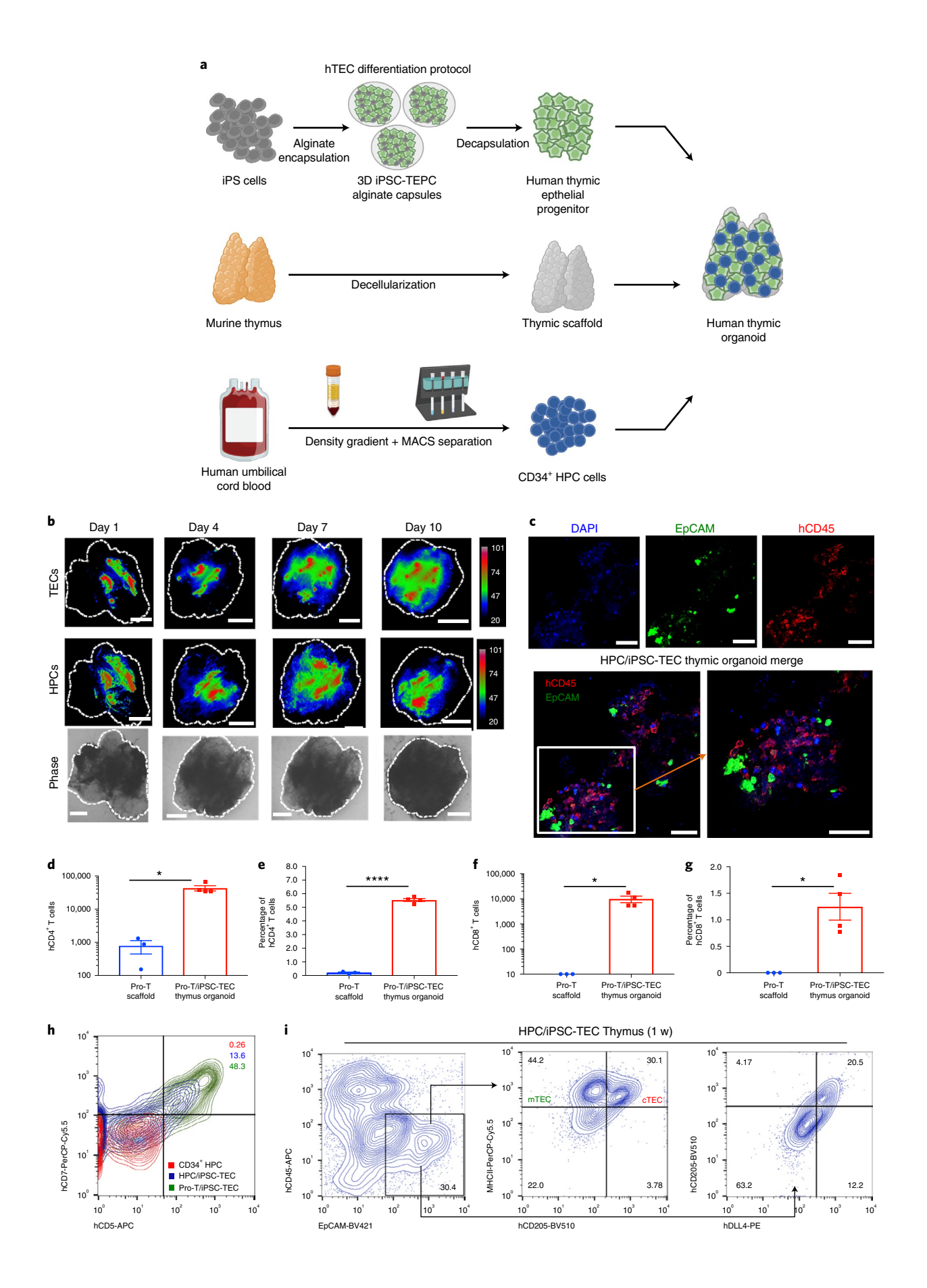
as well as those associated with epithelial-mesenchymal transition, such as *SNAI1* and *TWIST1*. This hybrid epithelial-mesenchymal phenotype is shared by both the in vitro expanded, clonogenic TEC cell lines and the freshly isolated 'common' TEC subsets (comTEC), recently reported by Campinoti and colleagues (Extended Data Fig. 3b and Supplementary Fig. 7)<sup>21</sup>. Finally, cells in combined cluster 2, which only contain cells from the 3D iPSC-TEC, express higher levels of cTEC and its progenitor genes (for example, *LY75*, *ITGA6* and *HLA-DPB1*), and lower levels of mesenchymal lineage markers (for example, *COL1A1* and *MMP2*), when compared to common cluster 1.

Phenotypic similarities between 2D TEC-0 and 3D TEC-0, as well as 2D TEC-1 and 3D TEC-2 clusters were further demonstrated by Kyoto Encyclopedia of Genes and Genomes (KEGG) pathway enrichment analysis, which showed that they share ten and 11 of the top 20 pathways associated with key cellular and biological functions, respectively (Supplementary Fig. 8). Moreover, both of the 2D TEC-1 and 3D TEC-2 clusters share five or more of the top 20 (KEGG) pathways with comTEC cells. Taken together, these data indicate that both 2D- and 3D iPSC-TECs share similar key transcriptional features as those of human TECs and/or TEC cell lines, and that 3D culture encapsulation promotes the development of combined cluster 2, at the expense of combined cluster 1 cells.

iPSC-TEC thymus can support T cell development in vitro. To examine their ability to program T cell differentiation, we first injected iPSC-TECs with CD34+ HPCs (including HSCs, isolated from human umbilical cord blood) into decellularized mouse thymic scaffolds, to generate the HPC/iPSC-TEC thymus organoids<sup>20</sup> (Fig. 3a). The microenvironment of thymic scaffolds would support the survival of injected thymic cells for more than 1 week when cultured in vitro (Supplementary Fig. 9). To monitor the dynamic spatial distribution of cells within the scaffolds over time, iPSC-TECs and HPCs were labeled with infrared fluorescent dyes DiD and DiR, respectively, coinjected and imaged sequentially with the LI-COR imaging system for 10 days. Broad distribution of both iPSC-TECs and HPCs was observed within the scaffolds, followed by redistribution and expansion after extended culture, suggesting ongoing remodeling of the thymus organoids (Fig. 3b and Supplementary Fig. 10). Notably, DiD and DiR signals were largely overlapping throughout the culture, suggesting the colocalization of CD45+ hematopoietic lineage cells with EpCAM+ TEPCs within the scaffold. Close interactions between TEPCs and CD45+ hematopoietic lineage cells were further demonstrated by immunofluorescence analysis, as shown in Fig. 3c.

It has been shown that crosstalk between TECs and progenitors of T cells (Pro-T, including TSPs and early thymic precursors (ETPs)) within the thymus are critical for T-lineage specification while synergistically promoting their mutual maturation<sup>32,34</sup>. To model thymic

**Fig. 3 | iPSC-thymus organoids can support the progression of T cell program in vitro. a**, Schematic illustration of human iPSC-thymus organoid construction. iPSC-TECs were coinjected with either CD34+ HPCs or Pro-T cells into decellularized mouse thymus scaffolds to generate HPC/iPSC-TEC or Pro-T/iPSC-TEC thymus organoids, respectively. **b**, L1-COR imaging of whole scaffolds showing changes in distribution of iPSC-TECs labeled with DiD (top row) and CD34+ HPCs labeled with DiR (middle row) over 10 days in culture. The boundary of the scaffold is shown as a white dotted line; white scale bar, 2 mm; color bars are a measure of signal intensity. The bottom row shows phase contrast images; scale bars 1 mm. Shown are representative of two independent experiments. **c**, Immunofluorescent staining of HPC/iPSC-TEC thymus organoids after 2 weeks of culture. White scale bars, 50 μm. Bottom row shows merged image (lower left panel), with boxed insert displaying higher magnification within the lower right panel. Shown are representative of two independent experiments with similar results. **d-g**, Characterization of CD4+ and CD8+ T cell production from Pro-T/iPSC-TEC thymus organoids after 1 week of in vitro culture. 5 × 10<sup>5</sup> Pro-T cells were used to repopulate the thymus scaffolds either alone or with an equal number of iPSC-TECs. **d,f**, Numbers of CD4+ (**d**, *P* = 0.0055) and CD8+ T cells (**f**, *P* = 0.034) yield per scaffold after 1 week of in vitro culture. **e,g**, Percentages of CD4+ (**e**, *P* < 0.0001) and CD8+ (**g**, *P* = 0.0087) cells in culture. Data are presented as mean values ±s.e.m. using a two-tailed unpaired *t*-test. **h**, Overlay of FCM plots to compare surface expression of T-lineage marker CD7 and CD5: red, CD34+ HPCs; blue, 1 week-cultured HPC/iPSC-TEC thymus organoids and green, 1 week-cultured Pro-T/iPSC-TEC thymus organoids. Shown are representative plots from three independent experiments with similar results. **i**, FCM analysis of TEC subset marker expression in 1 week-cultured HPC/iPSC-TEC thymus o



crosstalk and to demonstrate that the iPSC-TECs can support the progression of T cell program within the thymus scaffold microenvironments in vitro, we induced the differentiation of CD34+HPCs into Pro-T cells (Supplementary Fig. 11), and coinjected them into the thymus scaffold with the iPSC-TECs to construct the Pro-T/ iPSC-TEC thymus organoids. After 1 week of culture, a substantial population of cells progressed into CD3+CD4+CD8+ double positive, CD3+CD4+CD8- and CD3+CD4-CD8+ single positive stages of T cell development (Extended Data Fig. 4a, lower panels). In contrast, a small population of CD4 single positive cells was observed in thymic scaffolds repopulated with Pro-T cells alone (Pro-T scaffold, Extended Data Fig. 4a, upper panels), likely representing the immature single positive (ISP) CD4+ cell population35. Characterization of the emigrant population of the Pro-T/iPSC-TEC thymus organoids showed the presence of both CD3+TCRαβ+CD4+ and CD3+TCRαβ+CD8+ T cells (Fig. 3d-g and Extended Data Fig. 4b). Significantly higher numbers of CD4<sup>+</sup> T cells (over 50 times) were generated from the Pro-T/iPSC-TEC thymus organoids in comparison to the Pro-T scaffold controls (Fig. 3d). In comparison to CD4+ T cells, relatively lower amounts of CD8+ T cells were produced in the Pro-T/iPSC-TEC thymus culture and essentially no CD8+ T cells were detected in Pro-T scaffold controls (Fig. 3f). These findings suggest that Pro-T/iPSC-TEC thymus organoids can support the development of both CD4+ and CD8+ T cells in vitro.

Similar progression of early T cell program, albeit delayed, was observed in iPSC-TEC thymus organoids constructed with CD34<sup>+</sup> HPCs. After 1 week of in vitro culture, a small but prominent population of CD5<sup>+</sup>CD7<sup>+</sup> cells was present, suggesting ongoing T-lineage restriction and specification of the CD34<sup>+</sup> HPCs (Fig. 3h). While delayed in T cell development in comparison to those of Pro-T/iPSC-TEC thymus, continuous culture of HPC/iPSC-TEC thymus organoids after 2 weeks also supported the generation of both double positive and single positive thymocytes (Supplementary Fig. 12). These findings suggest that the microenvironments of iPSC-TEC thymus organoids induce the seeded progenitor cells to undergo T cell programming and have the potential to support the generation of CD4<sup>+</sup> and CD8<sup>+</sup> T cells in vitro.

Further maturation of iPSC-TECs into TEC subsets was also observed. RT-qPCR analyses of HPC/iPSC-TEC thymus organoids show significant increases in expression of both *MHCII* and *CD74*, genes that are essential for TECs to present self-antigens to mediate both positive and negative selection of developing T cells (Supplementary Fig. 13). Characterization of CD45<sup>-</sup>EpCAM<sup>+</sup> cells with FCM revealed the presence of both the MHCII<sup>+</sup>CD205<sup>+</sup>DLL4<sup>+</sup>cTEC and MHCII<sup>+</sup>CD205<sup>-</sup> mTEC subsets (Fig. 3i). These data indicate that successful thymic crosstalk can be established in iPSC-TEC thymus organoids, which synergistically promotes the maturation of iPSC-TECs into functional TEC subsets and the development of human T cells in vitro.

**iPSC-TEC thymus can support T cell development in vivo.** To investigate their capability to support T cell development in vivo, HPC/iPSC-TEC thymus organoids were transplanted underneath the kidney capsules of CD34<sup>+</sup> HPC-engrafted hu.SRC mice to

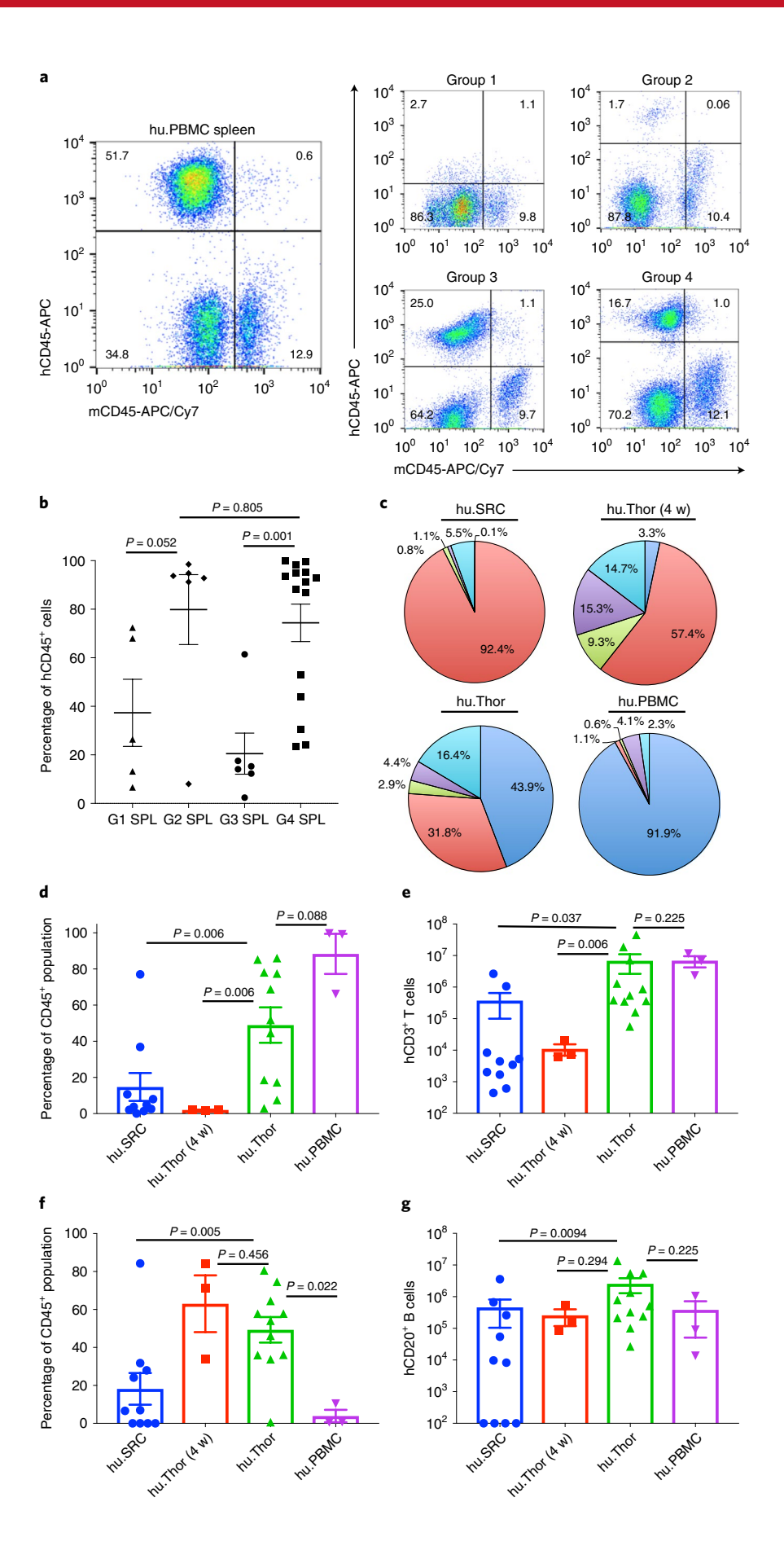
generate the humanized thymus organoid-engrafted (hu.Thor) mice (Extended Data Fig. 5a). The myeloablative alkylating agent busulfan was used to chemically precondition the NSG recipients before HPC and thymus organoid transplantation (group 2 in Extended Data Fig. 5a, with group 1 as control). As it has been shown, treating mice with anti-c-kit antibodies can deplete endogenous murine HSCs in the bone marrow and facilitate donor stem cell engraftment<sup>36</sup>, a c-kit depletion regimen was also evaluated (Extended Data Fig. 5a, group 4 for HPCs and HPC/iPSC-TEC thymus organoid transplantation, with HPC-engrafted group 3 as control). To ensure that human T cells generated from the iPSC-derived thymus organoids were functionally compatible with the HSC-derived APCs (for example, dendritic cells, macrophages and B cells), only CD34+ HPCs isolated from umbilical cord blood samples carrying partially matched human leukocyte antigen (HLA) alleles with the iPSCs were used in the study, unless otherwise stated (Supplementary Table 1). No signs of GVHD, such as decreased body weight, hair loss or lymphocytic infiltration of organs and tissues, were observed in hu. Thor mice after more than 350 days in the study (personal observation), suggesting mutual tolerance between the engrafted hCD34+ human hematopoietic lineage cells and those of the NSG recipients.

Robust and long-term human cell chimerism was observed in the blood, bone marrow and spleen of hu. Thor mice (Fig. 4a,b and Extended Data Figs. 5b and 6). Since group 4 mice displayed overall increased engraftment of hCD45+ cells over those of group 2 and controls, group 4 protocol was followed to generate hu. Thor mice for further characterization of the effects of iPSC-derived thymus organoid transplantation on human T cell development. To assess the function of T cells in hu. Thor mice, cohorts of hu. PBMC mice, in which preconditioned NSG mice were transplanted with mature and functional blood mononuclear cells, were generated and used as positive controls.

As early as 4 weeks post-transplantation, development of both lymphoid and myeloid lineage cells in the human hematopoietic compartment were detected in hu.Thor mice (Extended Data Figs. 6 and 7). Notably, CD20<sup>+</sup> B cells represented the predominant population of lymphocytes, in line with previous reports of delayed T cell development in thymus transplantation recipients. The development of CD45<sup>+</sup>CD3<sup>+</sup> T cell compartment, including both CD4<sup>+</sup> and CD8<sup>+</sup> subsets, became prominent in hu.Thor mice at 18–24 weeks postthymus and CD34<sup>+</sup> HPC transplantation (Fig. 4d–g and Extended Data Fig. 7).

To assess the de novo generated T cell compartment in hu. Thor mice, overall diversity of T cell populations were characterized by examining the expression of V $\beta$  and V $\alpha$  gene families with a NanoString T cell receptor (TCR) multiplex assay panel (Fig. 5a and Supplementary Fig. 14). Similar levels of reads for each V $\beta$  and V $\alpha$  family were detected in splenocytes of hu. Thor and hu. PBMC mice, as well as PBMCs from healthy human donors, demonstrating the potential of iPSC-TEC thymus organoid to support development of a complex T cell repertoire in hu. Thor mice. Further characterization of T-helper cells showed the presence of multiple subsets, such as those in hu. PBMC mice, including the CXCR3+CCR6-Th1, CXCR3-CCR6+Th17 and CXCR3-CCR6-Th2 cells, as well as

**Fig. 4 | Development of multiple hematopoietic lineages in hu.Thor mice.** Cells were isolated from spleens of hu.PBMC (n=4) and G1-G4 humanized mice (18-40 weeks post-transplantation, n=5-15 mice per group analysis) and analyzed with FCM for overall ratios of human cell chimerism (percentage of hCD45 in total CD45+ cells). **a**, Representative FCM graphs of splenocytes of hu mice from at least five independent experiments with similar results. **b**, Percentages of human hCD45+ cells in the spleens of G1 (n=5), G2 (n=6), G3 (n=6) and G4 (n=15) mice. Data are presented as mean values (middle line)  $\pm$ s.e.m. (error bars), using a two-tailed Mann-Whitney test, where P < 0.05 is considered as significance. SPL, spleen. **c**, Representative pie charts showing the distribution of human hematopoietic lineages of hu.SRC, early and late hu.Thor, and hu.PBMC mice. Shown are representative results from three independent experiments. **d**-**g**, Percentage and total number of CD3+ T cells (**d**,**e**, respectively) and CD20+ B cells (**f**,**g**, respectively) in the spleens of hu.SRC (n=10), early (4 weeks, n=3) and late hu.Thor (n=11), and hu.PBMC mice (n=3). Data are presented as scatter plots with bar graphs showing mean values n=5.e.m. (error bar) using a two-tailed Mann-Whitney test, where n=6.0.05 is considered as significance.



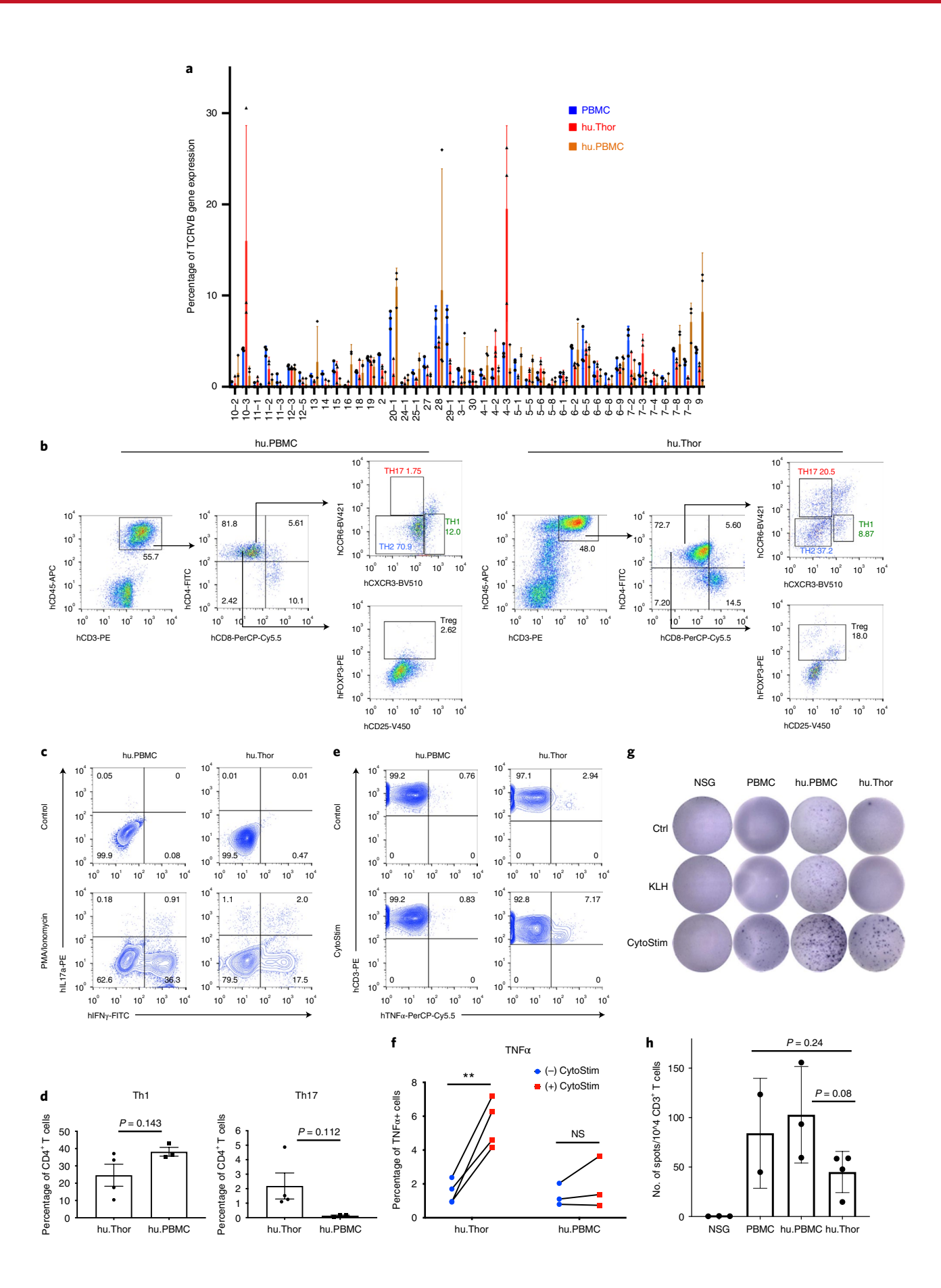


Fig. 5 | Development of functional human T cell subsets in hu.Thor mice. a, Overall diversity of TCR Vβ gene family. RNA was isolated from splenocytes of hu. Thor (red, n=3), hu. PBMC (brown, n=3) and PBMC of healthy donors (blue, n=3). V $\beta$  gene expression was analyzed with the NanoString T cell panel. Shown are the percentages of expression of each family over total TRBV genes. Data are denoted as mean ± s.d. (error bars). b, Splenocytes of hu. Thor (right panel, n = 4) and hu. PBMC mice (left panel, n = 3) were characterized with FCM for T cell subsets. Shown are representative graphs of CD4+ T-helper cells subsets (off hCD45+ gate). Similar results were obtained from analysis of other hu. Thor mice. c. Splenocytes of hu. Thor (right panels, n=4) and hu.PBMC (left panels, n=3) mice were stimulated with PMA plus ionomycin (lower panels) or dimethylsulfoxide control (upper panels) and intracellularly stained with antibodies against hIL17A and hIFNy. Shown are representative FCM graphs of CD4+T cells from two independent experiments with similar results. d, Percentages of IFNy-producing Th1 cells and IL17A-producing Th17 cells. Data are denoted as mean ± s.d. (error bars), using a two-tailed unpaired student t-test. e.f. Splenocytes and bone marrow cells were mixed at 1:1 ratio from hu. Thor (n=4) and hu. PBMC (n=3) mice, stimulated with CytoStim for 6 h, and intracellularly stained for TNFα. e, Representative FCM graphs showing hTNFα-producing hCD3<sup>+</sup> T cells, from at least three independent experiments with similar results. f, Percentages of TNF $\alpha$ -producing hCD3+ T cells before (blue dots) and after (red dots) CytoStim treatment. P = 0.0066 from a two-tailed, paired student t-test, where P < 0.05 is considered as significance. NS, not significant (P = 0.358), **g,h**, ELISpot analysis of IFNy-producing CD3<sup>+</sup> T cells, using mixture of splenocytes and bone marrow cells (1:1 ratio) of hu.Thor (n=4), hu.PBMC (n=3) and NSG (n=3) mice, or PBMC samples (n=2) from healthy donors. **g**, Representative ELISpot images of similar results from two independent experiments. 500,000 to 1 million cells were incubated overnight with medium (Ctrl), model antigen KLH and CytoStim. h, Normalized number of IFNγ-producing spots per 104 CD3+ T cells. Data are denoted as mean  $\pm$  s.d.

CD4<sup>+</sup>FoxP3<sup>+</sup> T-regulatory cells (Tregs), the critical population of CD4<sup>+</sup>T cells responsible for maintaining immune tolerance (Fig. 5b).

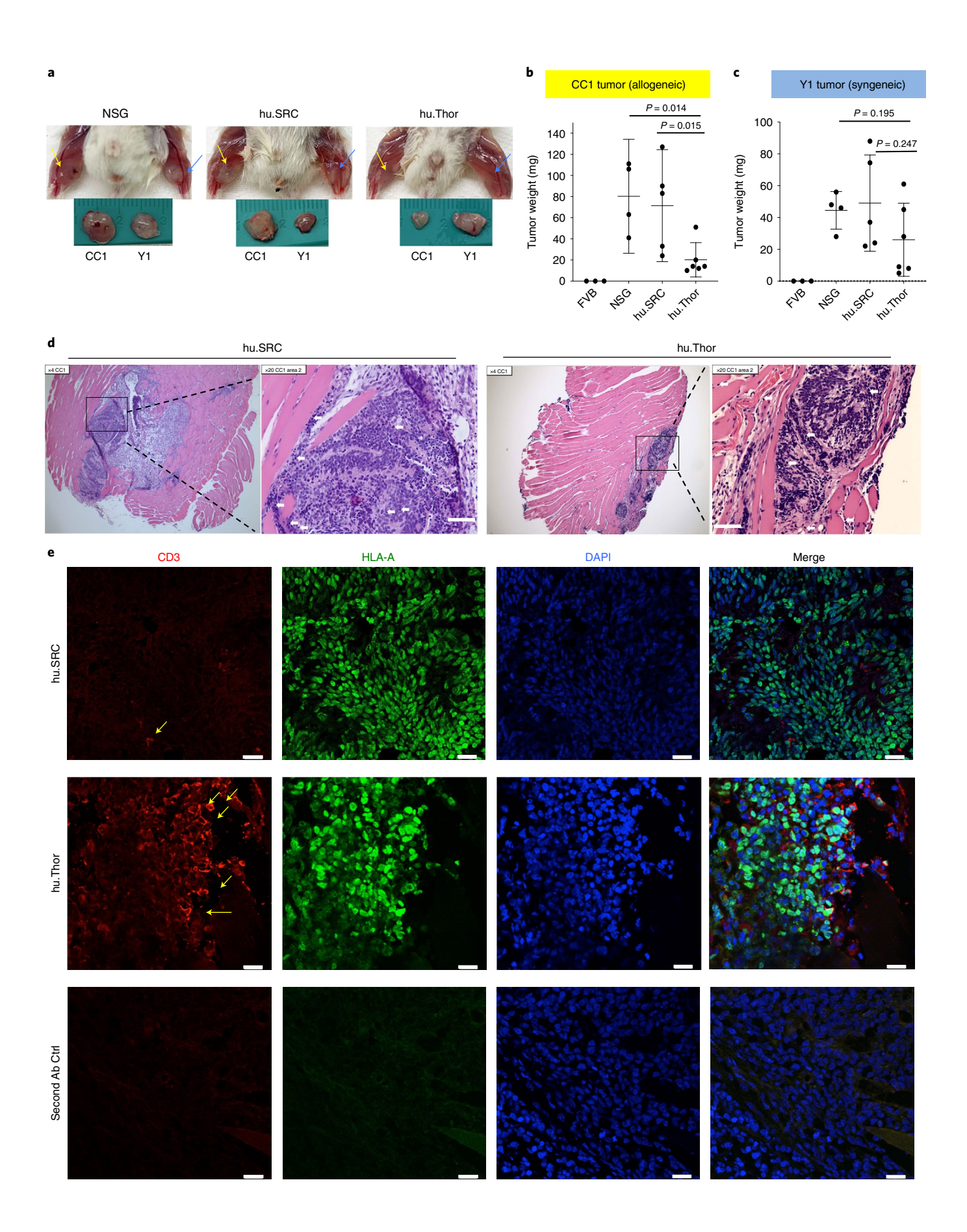
To demonstrate the function of key hu. Thor T cell subsets, hu. Thor T cells were stimulated with phorbol 12-myristate 13-acetate (PMA)/ ionomycin, intracellularly stained with anti-IFNy and anti-IL-17a antibodies and analyzed with FCM. Comparable with hu.PBMC splenocytes, both IFNγ-producing Th1 and IL-17a-producing Th17 cells were readily detectable, indicating the successful development of multiple functional T-helper lineages in hu. Thor mice (Fig. 5c,d). To further demonstrate that hu. Thor T cells can mediate antigen-specific immune responses, immune cells from spleens and bone marrows of hu. Thor mice were isolated, mixed at 1:1 ratio and challenged with CytoStim, an antibody-based, T cell activating reagent that acts similarly to superantigens by crosslinking TCRs to pMHC molecules on the surface of antigen presenting cells (APCs). Intracellular cytokine staining assays showed increased production of TNFα and IL-2 as early as 6 hours after stimulation (Fig. 5e,f and Extended Data Fig. 9a,b), whereas IFNy-producing cells became more prominent after overnight stimulation, as shown in ELISpot analysis (Fig. 5g,h). These findings are consistent with previous reports that TNFα-production predominates the early responses of naive T cells on antigen-stimulation (6h), while IFNy-secretion represents the relatively later stage of T cell action (overnight)<sup>37</sup>. In contrast, T cells of hu.PBMC mice displayed prominent IFNy responses even at early stage of activation (Extended Data Fig. 9c,d), since most of the cells had already adopted an effector and/or memory fate due to their previous exposure to murine cells and antigens. In line with these findings, a substantial number of IFNy-secreting cells were observed in control wells of hu.PBMC immune cells supplemented with either medium alone or naïve model antigen keyhole limpet hemocyanin (KLH), presumably due to the presence of mouse cells in the culture. Notably, such murine antigen-mediated xeno-immune reactivity was not detected in control cultures of hu. Thor cells, further indicating that the hu. Thor T cell compartments are tolerant toward the NSG hosts (Fig. 5g).

When challenged with allogeneic human cord blood cells that express HLA alleles totally mismatched with those of the engrafted CD34<sup>+</sup> HPCs and the iPSC-thymus organoids, hu.Thor T cells underwent robust proliferation responses (Supplementary Table 1 and Supplementary Fig. 15). Taken together, these results demonstrate that iPSC-derived thymus organoids can support the development of a diverse, functional and self-tolerant human T cell compartment in hu.Thor mice.

To further characterize hu.Thor T cells, gene expression profiling analyses were performed, focusing on pathways essential to T cell biology, such as T cell diversity, activation and TCR signaling. Hu. Thor immune cells exhibited similar overall T cell gene expression profiling as PBMCs from healthy donors, and cells of hu.PBMC mice, while differing from those of hu.SRC mice (Supplementary Fig. 16a). Specifically, both hu. Thor and hu. PBMC displayed higher levels of TCR diversity than hu.SRC, suggesting a more complex TCR repertoire (Supplementary Fig. 16b). Both hu.Thor and hu.PBMC also displayed higher TCR signaling and activation. Comparable pathway scores of T-helper subsets, such as Th1, Th2 and Treg cells, were observed between hu. Thor and hu. PBMC cells (Supplementary Fig. 16c). These phenotypic similarities between hu. Thor and hu. PBMC immune cells further highlight the capability of hu. Thor mice to recapitulate the molecular properties of human T cell-mediated immune pathways.

T cell-mediated allo-tumor rejection and Ig class switching. To further test the function of hu. Thor T cells in vivo, we challenged hu. Thor mice with teratomas derived from an allogeneic CC1 iPS cell line. Teratomas derived from Y1 iPS cells, from which the engrafted thymus organoids were generated, were used as syngeneic control. Dissociated small clusters of syngeneic Y1 and allogeneic CC1 stem cells were intramuscularly injected into the left and right hind limbs of hu. Thor mice, respectively. Teratomas were collected, measured and weighed at 3–4 weeks postinoculation (Fig. 6a–c). While robust growth of allogeneic CC1 teratomas was found in

**Fig. 6 | hu.Thor mice can effective reject allogeneic teratomas derived from iPSCs. a**, Representative photographic images of teratomas. Yellow and blue arrows indicate tumors derived from CC1 (n=5) and Y1 (n=6) iPSC lines, respectively. **b,c**, Weights of tumors derived from the CC1 (**b**, allogeneic) and Y1 (**c**, syngeneic) lines. Data are pooled from three independent experiments, and presented as mean values  $\pm$  s.d. using a two-tailed Mann-Whitney test. **d**, Histological images (H&E) of teratomas of allogeneic CC1 tumors in hu.SRC (left panels) and hu.Thor (right panels) mice. White arrows show the tumor infiltrating immune cells. Scale bars, 100 μm. Shown are representative images from tumors harvested from two hu.SRC and three hu.Thor mice. **e**, Immunofluorescent images of CC1 teratomas derived from hu.SRC (upper panels) and hu.Thor (mid panels) mice. Cryosections of teratomas were stained with anti-CD3 (red, for T cells) and anti-HLA-A (green, for both iPSC-derived tumor cells and tumor infiltrating T cells) antibodies, and counterstained with 4,6-diamidino-2-phenylindole for nucleus (blue). Yellow arrows highlight some of the clusters of CD3+ tumor infiltrating T cells. Lower panels are control staining without primary antibodies. Shown are representative images from tumors harvested from two hu.SRC and three hu.Thor mice. Scale bars, 20 μm.



NSG and hu.SRC mice, significantly smaller tumors were found in hu.Thor mice (Fig. 6b). Histological examination revealed lymphocytic infiltration of CC1 tumors in both hu.SRC and hu.Thor mice (Fig. 6d, white arrows), which is consistent with previous reports<sup>38</sup>. Immunofluorescent analysis of teratoma sections showed increased infiltration of human CD3+ T cells in CC1 tumors harvested from the hu.Thor mice (Fig. 6e). These results indicate that hu.Thor T cells can effectively mount alloreactive immune responses to reject allogeneic iPSC-derived tumors. Of note, no significant difference of syngeneic Y1 tumor growth was observed between NSG, hu.SRC and hu.Thor mice (Fig. 6c), suggesting that Y1 thymus organoids may induce immune tolerance of syngeneic grafts in hu.Thor mice.

T cell-dependent activation of B cells plays important roles in both the primary and secondary humoral adaptive immune response. After initial antigen exposure, cytokines secreted by Th2 cells promote plasma cells to undergo immunoglobulin class switching, shifting from producing IgM to IgG, IgA or IgE. Recurrent antigen exposure promotes the further maturation of memory B cells to undergo V(D)J somatic hypermutation at the immunoglobulin loci to generate IgGs with higher affinities against the target antigens. Human antibody isotyping multiplex assays were performed to examine the levels of immunoglobulin classes and subclasses in the sera of hu. Thor mice, in comparison to hu. SRC controls. Major human immunoglobulin classes including IgG, IgM, IgA and IgE were detected in hu. Thor sera (Extended Data Fig. 10). Notably, significantly higher levels of IgM, total IgG and IgG subclasses (IgG1 and IgG3) were observed when compared to hu.SRC samples. These results indicate that human T cells generated from the engrafted iPSC-derived thymus organoids can facilitate B cell maturation and isotype switching function. To further evaluate their capability to mount effective humoral responses against specific antigens, hu. Thor mice were immunized with vaccines against diphtheria toxoid. ELISA assays showed the generation of diphtheria toxoid-specific IgGs after the initial immunization, as well as an overall increase after booster shot administration (Supplementary Fig. 17). These results further indicate that T-helper cells generated from iPSC-derived thymus organoids in hu. Thor mice promote the maturation of human B cells and can be used to model humoral responses of the human adaptive immune system.

#### Discussion

We reported here the successful tissue engineering of thymus organoids from human iPSC-derived TECs that can support the generation of human T cells both in vitro and in vivo. Two and three major clusters were identified by unbiased clustering analysis of scRNA-seq data in the 2D and 3D cultures, respectively, indicating the heterogeneity of the iPSC-TEC populations generated in vitro. The major cluster in both 2D and 3D samples expressed mTEC markers, suggesting mTEC-oriented specification. A population of iPSC-TECs displaying an epithelial/mesenchymal hybrid phenotype was generated under both the 2D and 3D culture conditions. These cells shared striking molecular signature similarities with 'common TECs', a population of human TEC subsets expressing both cTEC and mTEC markers that was recently identified by Campinoti and colleagues<sup>21</sup>. The authors postulated that these progenitor-like cells were the main contributors of the clonogenic TEC lines that can be expanded extensively in vitro and support human T cell development in vivo when engrafted in hu.SRC mice. The unique population of iPSC-TECs identified only in the 3D, but not the 2D culture, displayed decreased mesenchymal markers but increased expression of epithelial markers, especially those of cTECs (for example, PRSS16 and CD205), suggesting that the 3D alginate encapsulation environments might promote the specification of the 'hybrid' TEC progenitors into cTEC lineage. When introduced into the extracellular matrix microenvironment of decellularized thymus scaffolds, together with either CD34<sup>+</sup> HPCs or Pro-T cells, 3D

iPSC-TECs matured further into CD205+MHCII+DLL4+cTEC and CD205-MHCII+ mTECs, and were able to support the differentiation of hematopoietic progenitors into CD3+CD4+ and CD3+CD8+T cells in vitro, highlighting their thymopoiesis function.

Hematopoietic humanized mice are powerful small animal models for studying the human immune system. While substantial progress has been made to improve the engraftment and differentiation of multiple lineage immune cells, development of a functional human T cell compartment remains a challenge. Over the years, a number of efforts have been made to improve the generation of the human T cells in these mice. Transgenic expression of human SCF, GM-CSF and IL-3 in NSG-SGM3 mice promotes the stable engraftment of diverse hematopoietic lineages, including CD3+ T cells, CD19+ B cells and CD33+ myeloid cells<sup>39,40</sup>. The recently generated RG SKI hIL-6 mouse line (Rag2-/-Il2rg-/- $SIRP\alpha^{h/m}IL-6^{h/h}$ ), which expresses human IL-6, shows better support for survival of lymphoid lineage cells<sup>41</sup>. These mice develop larger thymus glands and higher numbers of T cells, suggesting that hIL-6 can promote thymopoiesis. Successful IgG class switching is also observed in antibody-producing B cells, suggesting effective T-helper function. Although transgenic expression of human cytokines/factors can boost the propagation and survival of human T cells, they remain reliant on mouse thymus microenvironments and murine MHCs for T cell education, compromising their capability to model human immune responses. Moreover, formation of functional immunological synapses depends on the interactions between human costimulatory molecules (for example, CD28 and CD40) on human T cells and their mouse ligands (for example, CD80/86 and CD40L) on mouse APCs in these mice, as developing T cells were positively selected by murine pMHCs in the endogenous murine thymus (MHC restriction), and will primarily interact with murine APCs. While transgenic expression of human HLA molecules in mouse cells can partially rescue these T cell education and antigen presentation defects, recapitulating the composition of human HLA genes in mouse is not practical as it is more complex than that of the mouse (for example, three MHCI and three MHCII genes in human versus two MHCI and one MHCII genes in mouse). In contrast, iPSC-derived TECs in thymus organoids of hu. Thor mice support the selection of human T cells within a human thymic microenvironment. Our data demonstrate the development of T-helper subsets, such as Th1 and Th17 cells, that can effectively mediate (super)antigen-specific responses on stimulation, further suggesting that hu. Thor mice are able to recapitulate human adaptive immunity.

While we have demonstrated the proof-of-principle that iPSC-thymus organoids can support the development of a human T cell compartment to mediate adaptive immune responses, further optimization will be needed, such as improving the iPSC-derived TEC differentiation and using a more effective conditioning regimen. For example, we used 8–12-week old NSG mice as recipients in the study to limit the development of human T cells in endogenous mouse thymus glands, as it has been shown that the hypoplastic thymus glands in NSG mice undergo irreversible, age-associated fibrosis<sup>42</sup>. Indeed, we did not observe signs of recovery of endogenous mouse thymus in any hu. Thor mice examined. However, it has been shown that human cell engraftment is significantly more efficient in neonates than adult NSG mice<sup>43</sup>. Developing new preconditioning protocols will help to increase HSC colonization and human cell chimerism in adult NSG mice. Improving the survival and function of the engrafted iPSC-TEC thymus organoids is another area that requires further optimization. Although broad expression of both TCRVB and TCRVA genes were detected in hu. Thor mice, over representation of certain TCR V $\beta$  and V $\alpha$ families was observed, suggesting oligoclonal expansion. Such phenomena have been widely observed in immunocompromised mice with thymus-reconstitution<sup>44</sup>, presumably due to the homeostatic

expansion of de novo generated T cells in response to the lymphopenia environment. Treating hu.Thor mice with thymic trophic factors, such as growth hormone and keratinocyte growth factor<sup>45</sup>, will help to prolong the survival of the engrafted iPSC-TEC thymus organoids, enhance naïve T cell production and increase TCR repertoire complexity.

Another factor that might influence the overall human cell chimerism and T cell development in hu. Thor mice is the quality and quantity of the infused CD34+ HPCs. It was reported that the frequency of long-term HSCs (LT-HSCs), the stem cell population responsible for humanized mouse reconstitution, is highly variable between donors, ranging from 0.1 to 17.3% within the CD34<sup>+</sup> HPCs in umbilical cord blood samples<sup>46</sup>. At present, there is no consensus as to the markers that can be used to evaluate the in vivo hematopoiesis/engraftment function of CD34+ progenitor cells in humanized mice. To eliminate potential bias arising from different donors, efforts have been taken to generate both controls and hu. Thor mice with the same batch of CD34+ HPCs for comparison. Recently, Sauvageau and colleagues have shown that pyrimidoindole derivatives (for example, UM171) supports the robust expansion of cord blood LT-HSCs ex vivo while maintaining their self-renewal properties to support long-term engraftment<sup>47,48</sup>. These new protocols and associated markers are currently being evaluated to further expand LT-HSCs for hu. Thor mouse reconstitution43,49.

We used CD34<sup>+</sup> HPCs with partially matched HLA as the iPSC-TEC thymus organoids in the study. However, a fully matched HLA between the thymus organoids and the transplanted HSCs would better facilitate the recapitulation of human adaptive immunity in hu. Thor mice. Recently, it has been shown that CD34<sup>+</sup> HSCs with high in vivo engraftability and multi-lineage potential have been successfully generated from human iPSCs<sup>50–52</sup>. It is possible that humanized mice with both TEPCs and HSCs from a single patient can be achieved in the near future, which will further improve the modeling of the patient's adaptive immune system in small animals. Of note, no clinical signs of GVHD were observed during the life spans of the hu. Thor mice, some of which were kept alive for more than 12 months postengraftment, suggesting their long-term use.

In summary, our study suggests the feasibility of recapitulating T cell-mediated human adaptive immune responses from individual patients in iPSC-TEC thymus-engrafted humanized mouse models for long-term preclinical studies. Moreover, it is conceivable that, with further protocol improvement, artificial thymus could be bioengineered from a patient's own iPSCs for treatment of immune deficient disorders in the future.

#### Online content

Any methods, additional references, Nature Research reporting summaries, source data, extended data, supplementary information, acknowledgements, peer review information; details of author contributions and competing interests; and statements of data and code availability are available at https://doi.org/10.1038/s41592-022-01583-3.

Received: 22 September 2020; Accepted: 18 July 2022; Published online: 05 September 2022

#### References

- Mestas, J. & Hughes, C. C. Of mice and not men: differences between mouse and human immunology. J. Immunol. 172, 2731–2738 (2004).
- Shultz, L. D. et al. Humanized mouse models of immunological diseases and precision medicine. *Mamm. Genome* 30, 123–142 (2019).
- Walsh, N. C. et al. Humanized mouse models of clinical disease. Annu Rev. Pathol. 12, 187–215 (2017).
- Ito, R., Takahashi, T., Katano, I. & Ito, M. Current advances in humanized mouse models. Cell Mol. Immunol. 9, 208–214 (2012).
- Melkus, M. W. et al. Humanized mice mount specific adaptive and innate immune responses to EBV and TSST-1. Nat. Med. 12, 1316–1322 (2006).

 Lan, P., Tonomura, N., Shimizu, A., Wang, S. & Yang, Y. G. Reconstitution of a functional human immune system in immunodeficient mice through combined human fetal thymus/liver and CD34+ cell transplantation. *Blood* 108, 487–492 (2006).

- Shultz, L. D. et al. Human lymphoid and myeloid cell development in NOD/LtSz-scid IL2R gamma null mice engrafted with mobilized human hemopoietic stem cells. *J. Immunol.* 174, 6477–6489 (2005).
- Boehm, T. & Bleul, C. C. Thymus-homing precursors and the thymic microenvironment. *Trends Immunol.* 27, 477–484 (2006).
- Hedrick, S. M. Thymus lineage commitment: a single switch. *Immunity* 28, 297–299 (2008).
- Klein, L., Hinterberger, M., Wirnsberger, G. & Kyewski, B. Antigen presentation in the thymus for positive selection and central tolerance induction. *Nat. Rev. Immunol.* 9, 833–844 (2009).
- Klein, L., Kyewski, B., Allen, P. M. & Hogquist, K. A. Positive and negative selection of the T cell repertoire: what thymocytes see (and don't see). *Nat. Rev. Immunol.* 14, 377–391 (2014).
- Anderson, G. & Takahama, Y. Thymic epithelial cells: working class heroes for T cell development and repertoire selection. *Trends Immunol.* 33, 256–263 (2012).
- Ohigashi, I., Kozai, M. & Takahama, Y. Development and developmental potential of cortical thymic epithelial cells. *Immunol. Rev.* 271, 10–22 (2016).
- Klug, D. B. et al. Interdependence of cortical thymic epithelial cell differentiation and T-lineage commitment. Proc. Natl Acad. Sci. USA 95, 11822–11827 (1998).
- Mizuochi, T., Kasai, M., Kokuho, T., Kakiuchi, T. & Hirokawa, K. Medullary but not cortical thymic epithelial cells present soluble antigens to helper T cells. J. Exp. Med. 175, 1601–1605 (1992).
- Derbinski, J., Schulte, A., Kyewski, B. & Klein, L. Promiscuous gene expression in medullary thymic epithelial cells mirrors the peripheral self. *Nat. Immunol.* 2, 1032–1039 (2001).
- 17. Hinterberger, M. et al. Autonomous role of medullary thymic epithelial cells in central CD4(+) T cell tolerance. *Nat. Immunol.* 11, 512–519 (2010).
- Tajima, A., Pradhan, I., Geng, X., Trucco, M. & Fan, Y. Construction of thymus organoids from decellularized thymus scaffolds. *Methods Mol. Biol.* 1576, 33–42 (2019).
- Hun, M. et al. Native thymic extracellular matrix improves in vivo thymic organoid T cell output, and drives in vitro thymic epithelial cell differentiation. *Biomaterials* 118, 1–15 (2017).
- Fan, Y. et al. Bioengineering thymus organoids to restore thymic function and induce donor-specific immune tolerance to allografts. *Mol. Ther.* 23, 1262–1277 (2015).
- Campinoti, S. et al. Reconstitution of a functional human thymus by postnatal stromal progenitor cells and natural whole-organ scaffolds. *Nat. Commun.* 11, 6372 (2020).
- Shi, Y., Inoue, H., Wu, J. C. & Yamanaka, S. Induced pluripotent stem cell technology: a decade of progress. *Nat. Rev. Drug Disco.* 16, 115–130 (2017).
- Parent, A. V. et al. Generation of functional thymic epithelium from human embryonic stem cells that supports host T cell development. *Cell Stem Cell* 13, 219–229 (2013).
- Sun, X. et al. Directed differentiation of human embryonic stem cells into thymic epithelial progenitor-like cells reconstitutes the thymic microenvironment in vivo. Cell Stem Cell 13, 230–236 (2013).
- Okabe, M., Ito, S., Nishio, N., Tanaka, Y. & Isobe, K. Thymic epithelial cells induced from pluripotent stem cells by a three-dimensional spheroid culture system regenerates functional T cells in nude mice. *Cell Reprogram.* 17, 368–375 (2015).
- Chhatta, A. R. et al. De novo generation of a functional human thymus from induced pluripotent stem cells. J. Allergy Clin. Immunol. 144, 1416–1419 e1417 (2019).
- Ramos, S. A. et al. Generation of functional human thymic cells from induced pluripotent stem cells. J. Allergy Clin. Immunol. https://doi.org/ 10.1016/j.jaci.2021.07.021 (2021)
- Richardson, T., Kumta, P. N. & Banerjee, I. Alginate encapsulation of human embryonic stem cells to enhance directed differentiation to pancreatic islet-like cells. *Tissue Eng. Part A* 20, 3198–3211 (2014).
- Bredenkamp, N. et al. An organized and functional thymus generated from FOXN1-reprogrammed fibroblasts. *Nat. Cell Biol.* 16, 902–908 (2014).
- Rodewald, H.-R. Thymus organogenesis. *Annu. Rev. Immunol.* 26, 355–388 (2008).
- Bonfanti, P. et al. Microenvironmental reprogramming of thymic epithelial cells to skin multipotent stem cells. *Nature* 466, 978–982 (2010).
- Park, J.-E. et al. A cell atlas of human thymic development defines T cell repertoire formation. Science https://doi.org/10.1126/science.aay3224 (2020)
- Takahama, Y., Ohigashi, I., Baik, S. & Anderson, G. Generation of diversity in thymic epithelial cells. *Nat. Rev. Immunol.* 17, 295–305 (2017).
- Irla, M. in Thymus Transcriptome and Cell Biology (ed. Passos, G. A.) 149–167 (Springer International Publishing, 2019).

- Rothenberg, E. V. Single-cell insights into the hematopoietic generation of T-lymphocyte precursors in mouse and human. *Exp. Hematol.* https://doi. org/10.1016/j.exphem.2020.12.005 (2021).
- Czechowicz, A., Kraft, D., Weissman, I. L. & Bhattacharya, D. Efficient transplantation via antibody-based clearance of hematopoietic stem cell niches. Science 318, 1296–1299 (2007).
- Brehm, M., Daniels, K. & Welsh, R. Rapid production of TNF-alpha following TCR engagement of naive CD8 T cells. J. Immunol. 175, 5043–5049 (2005).
- Kooreman, N. G. et al. Alloimmune responses of humanized mice to human pluripotent stem cell therapeutics. Cell Rep. 20, 1978–1990 (2017).
- Jangalwe, S., Shultz, L. D., Mathew, A. & Brehm, M. A. Improved B cell development in humanized NOD-scid IL2Rγnull mice transgenically expressing human stem cell factor, granulocyte-macrophage colony-stimulating factor and interleukin-3. *Immun. Inflamm. Dis.* 4, 427–440 (2016).
- Billerbeck, E. et al. Development of human CD4+FoxP3+ regulatory T cells in human stem cell factor-, granulocyte-macrophage colony-stimulating factor-, and interleukin-3-expressing NOD-SCID IL2Rγnull humanized mice. *Blood* 117, 3076–3086 (2011).
- Yu, H. et al. A novel humanized mouse model with significant improvement of class-switched, antigen-specific antibody production. *Blood* 129, 959–969 (2017).
- 42. Brehm, M. A. et al. Parameters for establishing humanized mouse models to study human immunity: analysis of human hematopoietic stem cell engraftment in three immunodeficient strains of mice bearing the IL2rgamma(null) mutation. Clin. Immunol. 135, 84–98 (2010).
- Fares, I. et al. EPCR expression marks UM171-expanded CD34+ cord blood stem cells. Blood 129, 3344–3351 (2017).
- Khosravi-Maharlooei, M. et al. Cross-reactive public TCR sequences undergo positive selection in the human thymic repertoire. *J. Clin. Invest.* 129, 2446–2462 (2019).

- Rossi, S. W. et al. Keratinocyte growth factor (KGF) enhances postnatal T-cell development via enhancements in proliferation and function of thymic epithelial cells. *Blood* 109, 3803–3811 (2007).
- Mantri, S. et al. CD34 expression does not correlate with immunophenotypic stem cell or progenitor content in human cord blood products. *Blood Adv.* 4, 5357–5361 (2020).
- Fares, I. et al. Cord blood expansion. Pyrimidoindole derivatives are agonists of human hematopoietic stem cell self-renewal. *Science* 345, 1509–1512 (2014).
- 48. Cohen, S. et al. Hematopoietic stem cell transplantation using single UM171-expanded cord blood: a single-arm, phase 1–2 safety and feasibility study. *Lancet Haematol.* 7, e134–e145 (2020).
- Tomellini, E. et al. Integrin-α3 Is a functional marker of ex vivo expanded human long-term hematopoietic stem cells. *Cell Rep.* 28, 1063–1073.e1065 (2019).
- Tan, Y.-T. et al. Respecifying human iPSC-derived blood cells into highly engraftable hematopoietic stem and progenitor cells with a single factor. *Proc. Natl Acad. Sci. USA* 115, 2180–2185 (2018).
- 51. Hoggatt, J. et al. Rapid mobilization reveals a highly engraftable hematopoietic stem cell. *Cell* 172, 191–204.e110 (2018).
- 52. Sugimura, R. et al. Haematopoietic stem and progenitor cells from human pluripotent stem cells. *Nature* **545**, 432–438 (2017).

**Publisher's note** Springer Nature remains neutral with regard to jurisdictional claims in published maps and institutional affiliations.

Springer Nature or its licensor holds exclusive rights to this article under a publishing agreement with the author(s) or other rightsholder(s); author self-archiving of the accepted manuscript version of this article is solely governed by the terms of such publishing agreement and applicable law.

© The Author(s), under exclusive licence to Springer Nature America, Inc. 2022

#### Methods

**Ethical statement.** All the works in the study were reviewed and approved by the Institutional Review Board at Allegheny Singer Research Institute of Allegheny Health Network (protocol nos. 1055-2-IACUC and IBC-132-AGH).

Mice. All animal procedures were performed with approval from the Allegheny Health Network Institutional Animal Care and Use Committee. All mice were housed in specific pathogen-free facility. Both NOD.Cg.*Prkdcwid1l2rgmi1vjl/SzJ* (NSG) and Friend virus B mice were purchased from the Jackson Laboratory. NSG mice were 8–12-week old on the date of thymus transplantation. The 3–4 week old CD-1 mice were purchased from Charles River. Mice are housed in optimal environmental conditions, including a 14-h light/10-h dark cycle, 18–24 °C temperature and 40–60% humidity.

Alginate encapsulation of single-cell iPSCs for induction of differentiation.

Alginate encapsulation of iPSCs has been previously described  $^{53}$ . Single-cell iPSCs were formed by pretreating a confluent cell population with  $10\,\mu M$  Y-27632 dihydrochloride (R&D Systems) 2h before dissociating with Accutase (StemPro). Cells were counted using Trypan Blue (Gibco) and a hemocytometer. Single cells were suspended in 1.1 w/v% low viscosity alginate (Sigma) at a cell density of  $5\times10^5$  per ml alginate. The single-cell alginate mixture was polymerized dropwise with a stirred solution of  $100\, mM$  CaCl $_2$  (Sigma) with  $10\, mM$  HEPES forming spherical capsules. The capsules were washed three times with DMEM/F12 (Gibco) before culturing in mTeSR1 (StemCell Technologies) supplemented with  $10\, \mu M$  Y-27632 dihydrochloride for 4–6 days before starting differentiation.

Differentiation of iPSCs into thymic epithelial progenitor cells (iPSC-TECs) and islet progenitor cells in 3D alginate capsules. The stage-wise induction protocol for thymic epithelial progenitor differentiation of hESCs was adopted from a previous study $^{23}$ . Stage 1 for definitive endoderm was carried out with Melton beta cell differentiation protocol. Stage 2 for anterior foregut endoderm was carried out in Roswell Park Memorial Institute (RPMI) media supplemented with 0.5% B27 (Gibco). For stage 2 (anterior foregut endoderm), the following factors were used:  $100\,\mathrm{ng}\,\mathrm{ml}^{-1}$  Activin A on day 5, 0.25  $\mu\mathrm{M}$  retinoic acid on days 5–7,  $50\,\mathrm{ng}\,\mathrm{ml}^{-1}$  BMP4 (Miltenyi Biotec) on days 6–7 and  $5\,\mu\mathrm{M}$  LY364947 (MilliporeSigma) on days 6–7. Stages 3 and 4 for VPE and thymic epithelial progenitor were carried out in DMEM/F12 media (Gibco) supplemented with 0.5% B27. For stages 3 (VPE) and 4 (TEP), the following factors were used:  $50\,\mathrm{ng}\,\mathrm{ml}^{-1}$  Wnt3A on days 8–11,  $0.1\,\mu\mathrm{M}$  retinoic acid on days 8–11,  $50\,\mathrm{ng}\,\mathrm{ml}^{-1}$  BMP4 on days 8–11,  $5\,\mu\mathrm{M}$  LY364947 on days 8–9,  $50\,\mathrm{ng}\,\mathrm{ml}^{-1}$  FGF8b (Miltenyi Biotec) on days 8–11 and  $0.5\,\mu\mathrm{M}$  KAAD-cyclopamine (Millipore) on days 8–11.

iPSC encapsulation and differentiation into islet progenitors were described previously<sup>53</sup>. Briefly, three base media were used in the islet cell induction process: stage 1 (S1): 2.44 mM D-glucose, 2.46 gl<sup>-1</sup> NaHCO<sub>3</sub>, 1:50 ITS-X, 0.25 mM vitamin C, 2% FAF-BSA, 2 mM glutamax, 1% penicillin/streptomycin (pen/strep), 490 ml MCDB131 media; stage 2 (S2): 2.44 mM D-glucose, 1.23 gl<sup>-1</sup> NaHCO<sub>3</sub>, 1:200 ITS-X, 0.25 mM vitamin C, 2% FAF-BSA, 2 mM glutamax, 1% pen/strep, 490 ml of MCDB131 media; Stage 3 (S3): 2.44 mM D-glucose, 2.98 gl<sup>-1</sup> NaHCO<sub>3</sub>, 1:200 ITS-X, 0.25 mM vitamin C, 2% FAF-BSA, 20 mM glutamax, 1% pen/strep, 490 ml MCDB131 media

Growth factors included into the base media depending on the day of differentiation are as follows: days 1-3 (definitive endoderm) include  $1.4\,\mu g\,ml^{-1}$  Chir99021 (day 1 only) and  $100\,ng\,ml^{-1}$  Activin A in the S1 media. Days 4 and 6 (Primitive Gut Tube) include  $50\,ng\,ml^{-1}$  KGF in the S2 media. Days 7 and 8 (Pancreatic Progenitor 1) include  $50\,ng\,ml^{-1}$  KGF, 0.25  $\mu$ M Sant 1,  $2\,\mu$ M retinoic acid,  $500\,nM$  PdBU and  $10\,\mu$ M Y-27632 in S2 media. Days 9, 11 and 13 (Pancreatic Progenitor 2) supplement the S2 media with  $50\,ng\,ml^{-1}$  KGF, 0.25  $\mu$ M Sant 1,  $0.1\,\mu$ M retinoic acid,  $10\,\mu$ M Y-27632 and  $5\,ng\,ml^{-1}$  Activin A. Days 14 and 16 (Endocrine Progenitor 1) supplement the S3 media with  $0.25\,\mu$ M Sant 1,  $0.1\,\mu$ M retinoic acid,  $1\,\mu$ M XXI,  $10\,\mu$ M ALk5i II,  $1\,\mu$ M T3,  $20\,ng\,ml^{-1}$  Betacellulin, and  $10\,\mu g\,ml^{-1}$  Heparin. Days 18-30 (Endocrine Progenitor 2), supplement the S3 media with  $0.025\,\mu$ M retinoic acid,  $1\,\mu$ M XXI,  $10\,\mu$ M ALk5i II,  $1\,\mu$ M T3,  $20\,ng\,ml^{-1}$  Betacellulin, and  $10\,\mu g\,ml^{-1}$  Heparin. Days 18-30 (Endocrine Progenitor 2), supplement the S3 media with  $0.025\,\mu$ M retinoic acid,  $1\,\mu$ M XXI,  $10\,\mu$ M ALk5i II,  $1\,\mu$ M T3,  $20\,ng\,ml^{-1}$ Days 30-44 (Maturation) use S2 media without growth factor supplementation.

Hematopoietic humanized mouse construction and umbilical cord stem cell isolation. The presence of endogenous mouse thymus gland, while degenerated, might still compete with the engrafted thymus organoid for HSC homing. To limit its impact, we used 8–12-week old NSG mice as recipients, as it has been shown that the hypoplastic thymus glands in NSG mice undergo irreversible, age-associated fibrosis\*2. We did not observe signs of recovery of endogenous mouse thymus in any hu. Thor mice examined.

Hu.SRC mice were generated via transplanting conditioned NSG mice with human umbilical cord-derived CD34+ cells. In brief, certain recipient NSG mice were given 250  $\mu$ l of 2 mg ml $^{-1}$  antimouse CD117 (c-kit) antibody intraperitoneally (Biolegend) 1 week before transplant. At 48 and 24 h before infusion of human cord blood cells, all NSG mice involved in the study were given 25–30  $\mu$ g g $^{-1}$  of busulfan intraperitoneally (Sagent Pharmaceuticals). All the treated NSG mice were fed with antibiotics-supplemented drinking water (Baytril, 200  $\mu$ g ml $^{-1}$ ) 1 week before and 2 weeks after the procedure.

Human umbilical cord blood was purchased from Vitalant. Ficoll separation was used to separate the lymphocyte population from the blood and the CD34+ cell population was isolated via the human CD34 Microbead Kit UltraPure (Miltenyi Biotec) and confirmed using FCM staining for human CD45-APC (BD Biosciences) and human CD34-VioBlue (Miltenyi Biotec). Cells were then either forzen or cultured until transplant (less than 7 days). On the day of transplant,  $5 \times 10^3 - 1 \times 10^6$  CD34+ cells were injected retroorbitally into recipient mice.

To generate the hu.Thor mice, NSG mice were preconditioned as described above and infused with  $1-3\times10^5$  CD34+ HPCs (containing HSCs). Thymus organoids, constructed and cultured as described below, were transplanted on the same day. Recipient mice were anesthetized with isofluorane and the thymus organoid was transplanted beneath the left kidney capsule. Data presented in the study were from hu.Thor mice engrafted with the HPC/iPSC-TEC thymus organoids. Similar findings were observed in hu.Thor mice engrafted with Pro-T/iPSC-TEC thymus organoids.

Generation of human HPC/iPSC-TEC and Pro-T/iPSC-TEC thymic organoids. Murine thymus decellularization was achieved with chemical detergent washing method as previously described<sup>28</sup>. In brief, thymic glands were harvested from 3–4-week old CD-1 mice and incubated in 0.1% SDS solution (Invitrogen) under continuous rotation at room temperature until the tissue was translucent (roughly 24h). The decellularized thymus glands were washed three times in phosphate-buffered saline (PBS) and subsequently incubated in 1% Triton X-100 (Sigma-Aldrich). After three more PBS washes, the organs were incubated in PBS plus pen/strep (100 U ml<sup>-1</sup>) and rotated for an additional 48h. The decellularized thymus scaffolds were stored in PBS with antibiotics at 4°C for up to 1 month.

Decellularized thymus scaffolds were reconstituted with isolated CD34+ umbilical cord blood cells and iPSC-TECs. To release iPSC-TECs from encapsulation, alginate capsules were gently pelleted (200g for 5 min) and incubated in 100 mM EDTA solution for 5 min at room temperature. After washing with PBE buffer (1× PBS+1%BSA+1 mM EDTA), cells were subjected to Ficoll-Paque gradient centrifugation (GE Healthcare Life Science) to remove alginate debris and dead cells (400g for 30 min at room temperature with brake off). Cells in the PBE/Ficoll interface layer were collected, rinsed three times with PBE and counted.

To construct the iPSC-TEC thymus organoids, 0.5–1 million of iPSC-TECs were mixed with CD34+ HPCs or in vitro generated Pro-T cells at 1–3:1 ratio, pelleted and resuspended in 40  $\mu$ l of StemSpan SFEM II base media supplemented (StemCell Technologies) with human SCF (100 ng ml $^{-1}$ ), human FLT3L (100 ng ml $^{-1}$ ), human TPO (50 ng ml $^{-1}$ ) (Miltenyi) and human keratinocyte growth factor supplement (ThermoFisher Scientific). The cells were then injected into both lobes of the thymic scaffold and cultured in either the upper chamber of the transwells for 5–7 days before transplant or 24-well tissue culture dish precoated with fibroblastic cells isolated from the lymph nodes (ScienCell Research Laboratories) for in vitro T cell generation. Both interleukin 2 (rhIL-2, 5 ng ml $^{-1}$ , Biolegend) and interleukin 7 (rhIL-7, 5 ng ml $^{-1}$ , Miltenyi Biotec) were supplemented to the in vitro T cell generation culture.

Pro-T cells were generated from differentiating CD34<sup>+</sup> HPCs isolated from umbilical cord blood using StemSpan lymphoid progenitor expansion medium and StemSpan lymphoid differentiation coating material (StemCell Technologies). Nontissue culture treated 24-well plates were coated with lymphoid differentiation coating material for 2h at room temperature and then washed three times with PBS. CD34<sup>+</sup> HPCs were plated and maintained at 10,000 cells per ml in lymphoid differentiation medium, with half of the medium changed every 3 days until day 14. Pro-T cells generated were either used for thymus organoid construction or cryopreserved for future use.

LI-COR imaging. iPSC-TECs and CD34+ HPCs were labeled with Vybrant lipophilic carbocyanine dyes DiD and DiR (ThermoFischer), respectively, following the manufacturer's suggested protocols. The labeled cells were admixed at 1:1 ratio and injected into the decellularized thymus scaffolds. Scaffolds thus recellularized were imaged using Odyssey infrared scanner (LI-COR Biosciences) periodically over a duration of 10 days in culture (days 1, 4, 7 and 10). The images were collected using Odyssey Image Studio with the highest possible sensitivity and resolution (21 µm) in 700 nm (DiD emission) and 800 nm channels (DiR emission). The images were analyzed using Fiji (ImageJ, National Institutes of Health) and the fluorescence intensity is represented as a heatmap of areas in the scaffold with cells. The heatmap was graded into three levels of cell density-low, moderate and high indicated by blue, green and red colors, respectively, based on the fluorescence intensity. Grayscale values in the range (20, 48) were designated with blue (low intensity), (48, 76) as green (moderate intensity) and (76, 101) as red (high intensity) and all levels below 20 are considered as background (black/no signal). The area fractions of images in both TEC and HPC density were extracted from the image data, normalized to total scaffold area from the phase images and compared over time in culture.

Murine peripheral blood collection and staining. Peripheral cheek blood was collected from transplanted mice and stained for markers of humanization and T cell generation. Murine facial veins were gently punctured with a 25 G needle and

blood was collected in heparin-coated microvette tubes and vials until processing. To process, blood volume was brought to approximately 1 ml using sterile PBS. Next,  $300\,\mu$ l of Ficoll-Paque solution was loaded into a 1.5 ml Eppendorf tube and the diluted blood mixture was slowly added on top of the Ficoll-Paque with care taken not to disturb the layer. The tube was then centrifuged at 400g for 20 min at room temperature with the brake set to 0. Once the spin was finished, approximately  $500-600\,\mu$ l of the upper, clear layer was removed and disposed. The white cellular layer located just above the Ficoll layer was then removed and placed in a clean polypropylene tube. PBE was added and tube was centrifuged at 400g for 5 min to wash the layer. Liquid was decanted slowly and cells were then placed into FCM staining protocol.

iPSC-TEC thymus organoid dissociation. To dissociate the thymus organoids cultured in vitro, an enzymatic digestion solution containing 0.4 mg ml collagenase D, 0.6 mg ml<sup>-1</sup> dispase II, 0.1 mg ml<sup>-1</sup> DNase I, 10 µM rock inhibitor was prepared using DMEM medium. Each thymus organoid was mechanically dissociated in 1 C tube with 2 ml of the digestion solution on gentleMACs Dissociator (Miltenyi Biotec). The dissociation was performed at 37 °C for 6 min under the program 37C-ABDK-02 for two rounds. At the end of the first round, the supernatant of the digestion reaction was collected, filtered and quenched with 4 ml of PBE. The remaining organoid was further dissociated under the same condition with 2 ml of fresh digestion solution. The supernatant was collected the same way and combined with the first round. The dissociated cells were pooled, pelleted and resuspended in 1 ml of culture medium for cell count and downstream analysis. For samples with suboptimal viability, density gradient centrifugation was performed to remove debris and dead cells as described above. Briefly, 1 ml of the cell suspension was laid gently onto 300 µl of Ficoll-Paque in a 1.5-ml Eppendorf tube and centrifuging at 1,600 r.p.m., room temperature for 20 min without brake. Live cells were collected at the medium/Ficoll interface and washed with fresh medium before proceeding to downstream analysis.

FCM analyses. Decapsulated TECs were stained with the following antibodies to determine their surface protein expression: antihuman CD45-APC, MHC Class II-PerCP-Cy5.5, EpCAM-BV421, CD205-BV510 (BD Biosciences) and DLL4-PE (Biolegend). All samples were compared to fluorochrome-matched IgG controls.

Blood was harvested from hu.Thor mice at various time points and processed as described above to determine both the humanization and T cell generation. Isolated live white blood cells were stained with the following antibodies: antihuman CD45-APC, CD3-PE, CD4-V450, CD8-FITC and antimouse CD45-PerCP-Cy5.5 (BD Biosciences) in V bottom-shaped 96-well microplates (Corning), fixed in 2% paraformaldehyde (PFA) and analyzed on a fluorescence-activated cell-sorting (FACS) Influx system (BD Biosciences). Humanized mice displaying less than 0.5% of hCD45+ cells in the peripheral blood at 12-weeks posthuman cell engraftment or at the time of the euthanasia were considered as graft failure and removed from the studies.

On days of animal euthanasia and tissue harvest, murine bone marrow and splenocytes were stained with the following additional antibodies: antihuman CD20-V450, CD14-PE, CD33-V450, CD45RA-PE, CD45RO-FITC, CD25-V450, CD11c-FITC, CD56-FITC, CD117-PE, TCR $\alpha$ P-PE, TCR $\gamma$ 8-FITC, CCR6-BV421 and CXCR3-BV510 (BD Biosciences). Antihuman FOXP3-PE was also stained for intracellularly with the FOXP3/Transcription Factor Staining Buffer set according to manufacturer's protocol (ThermoFisher). Additional information on the antibodies used can be found in Supplementary Table 2. Dead cells were excluded from analyses through the use of the LIVE/DEAD Violet Fixable dead cell stain kit (ThermoFisher). All corresponding FCM analyses were performed on FlowJo 10 (v.10.5.3) software.

Alignment and analysis of scRNA-seq data. Single cells were isolated from both 2D and 3D TEC samples. In brief, 2D TECs were removed from wells via trypsinization. Media was removed from the wells and TrypLE Select dissociation buffer (ThermoFisher) was added. Cells were then incubated at  $37\,^{\circ}\mathrm{C}$  for 7 min, after which cells were gently pipetted off the wells and any remaining aggregates were manually broken up. Cells were then placed in DMEM/F12 media supplemented with  $1\times$  B-27 (ThermoFisher) and Y-27632 Rock inhibitor (1:1,000, StemCell Technologies) and centrifuged at 250g for 5 min to pellet.

The 3D TECs were decapsulated with  $100\,\mathrm{mM}$  EDTA and placed in a Ficoll gradient to remove both capsular debris and dead cells as previously noted. The live cell layer was pipetted off the gradient to be dissociated for analysis. Live cellular aggregates were placed in DMEM/F12 media supplemented with  $1\times$  B-27 and Y-27632 Rock inhibitor and allowed to settle for  $10\,\mathrm{min}$ . Media was then gently removed and aggregates were placed in TrypLE Select and incubated for  $17\,\mathrm{min}$ . On completion, cells were centrifuged at 250g for  $5\,\mathrm{min}$  to pellet.

Once pelleted, cells were then checked for both viability as well as the presence of any remaining aggregates using the Counters II Automated Cell Counter (ThermoFisher). Single cells were then suspended in PBS supplemented with 20% FBS and sent to the Genomics Research Core at the University of Pittsburgh for quality control, library preparation and droplet sequencing on the 10X Genomics Chromium controller. Single cells (>70% viability) were washed, strained, and subjected to 10X Genomics single-cell library construction (Chromium single-cell

3' reagent v.3 kit) and sequencing protocol according to the manufacturer's recommendations.

The count files were demultiplexed and aligned using Cell Ranger pipeline. To cluster the cells in our datasets, we first compute principal component analysis projection for all cells, and construct the k-nearest neighbor graph of the cells based on Euclidean distances in principal component analysis space (with k= 20). We then use the Louvain algorithm to cluster our cells the granularity of the clusters is determined by a user-defined resolution parameter, and for both our 2D and 3D iPSC-TECs, we used a resolution of 0.1. These steps were all completed in R using Seurat.

To align the 2D and 3D iPSC-TEC datasets, scRNA-seq integration was performed following the approach described in Stuart et al. A set of 'anchor' pairs was identified between the two datasets, which are pairs of cells representing the same biological state in the two datasets. Anchors are computed in the reduced dimension space via canonical correlation analysis, which is used to identify pairs of mutual nearest neighbor cells. These anchors were calculated using the FindIntegrationAnchors function in Seurat. After identifying these anchors, a weighted average of vector differences between cells to be integrated and anchors is used to transform the representation of cells and produce a final integrated expression matrix. The integrated expression matrix that combines the 2D and 3D iPSC-TEC datasets was calculated using the IntegrateData function in Seurat. Cells were clustered again in this aligned dataset using the Louvain algorithm as described above, using the same resolution parameter of 0.1.

RNA isolation and gene expression analysis. Total RNA was extracted with TRIzol (Invitrogen) and complementary DNA was synthesized using the SuperScript III First-Strand synthesis system for RT-PCR (Invitrogen). Real-time qPCR was performed using the All-in-One qPCR Mix (Genecopoeia) with a Roche LightCycler 480 system (Roche Applied Science). Quantitative real-time PCR primer sequences used in this study are shown in Supplementary Table 3. PCR reactions were performed in triplicate in at least three separate experiments. Relative gene expression was normalized to GAPDH.

For gene expression profiling analysis, RNA was extracted from the splenocytes of hu. Thor and hu. SRC humanized mice using the TRIzol method (Invitrogen), following the manufacturer's protocol. The concentration, quality, and integrity of each RNA sample was examined first by Nanodrop Spectrophotometer, followed by Biolanalyzer 2100 (RNA Pico kit, Agilent). Only samples with DV200 values above than 70% were used in the study. 150-500 ng of total RNA was loaded to CAR-T cell gene profiling hybridization cartridge that can capture reporter probes for 771 genes (with unique barcode) specific to various pathways of T cell function, and was characterized with nCounter Max Gen 2 System (NanoString Technologies). Splenocytes isolated from NSG mice were used as negative control, in which less than 15% of the genes were above background and were excluded from the analysis. All reads were analyzed with nSolver v.4.0 Advanced analysis software. Specifically, pathway score analysis was carried out, which condense each sample's gene expression profile into a small set of pathway scores. Pathway scores are fit using the first principal component of each gene set's data. They are oriented such that increasing score corresponds to mostly increasing expression (specifically, each pathway score has positive weights for at least half its genes). Summary plots explore the joint behavior of pathways, and covariate plots compare pathway scores to covariates.

To characterize the TCR V $\beta$  gene family usage, total reads of V $\beta$  genes from the T cell gene panel were calculated and percentage of individual V $\beta$  family expression was calculated. The same method was used to calculate the usage of Vageve families.

T cell subset phenotyping. Splenocytes were collected from hu.Thor mice. Then  $1\times 10^6$  cells per ml were placed in RPMI-10 and plated in a nontissue culture treated six-well plate. Cells were stimulated with both ionomycin (1 µg ml $^{-1}$ ) and PMA (50 ng ml $^{-1}$ ) and treated with Golgi block as described in the Human Th1/Th17 Phenotyping Kit (BD Biosciences). Control wells were left unstimulated and unblocked. Cells were incubated at 37 °C for 5 h and then collected and pelleted in polypropylene FACS tubes. Cells were then resuspended in cold BD Cytofix buffer and incubated at room temperature. Cells were pelleted and washed in PBE and the resuspended in 1× BD Perm/Wash Buffer before incubation at room temperature. After a final centrifugation, cells were stained with the following antibody cocktail: antihuman CD4-PerCP/Cy5.5, IL-17A-PE, IFNy-FITC, CD45-APC and antimouse-APC/Cy7 (BD Biosciences). Cells were fixed in 2% PFA before FACS analysis.

Mixed lymphocyte reaction. hu.Thor mice were euthanized and their spleens and bone marrow were harvested. Splenocytes and bone marrow cells from the same animal were combined, counted and labeled with carboxyfluorescein succinimidyl ester (Invitrogen), except for a small portion that was set aside as unlabeled as a negative control. In brief,  $1\times 10^7-1\times 10^8$  hu.Thor responder cells were resuspended in a  $10\,\mu\text{M}$  working solution of carboxyfluorescein succinimidyl esterin PBS. Cells were incubated at  $37\,^{\circ}\text{C}$  while being kept protected from light and staining was quenched through the addition of RPMI-10 containing 10% FBS. Cells were then pelleted and resuspended in RPMI-10 and then left to incubate for 10 min.

A small fraction of these labeled cells were then Fc blocked (BD Biosciences) stained with the following antibodies to act as the positive control: antihuman CD45-APC, CD3-PE, CD4-PerCP/Cy5.5, CD8-BUV395 and Violet LIVE/DEAD (BD Biosciences). The remaining cells were counted and  $1-2\times10^5$  of these labeled responder cells were plated in triplicate in a 96-well round-bottomed plate.

Allogeneic stimulator cells were prepared from human umbilical cord blood samples using mitomycin-C treatment. In brief, CD34+ cells isolated from umbilical cord blood were cultured and counted. Cell suspensions were made at  $5 \times 10^7$  cells per ml in PBS. Mitomycin-C (Sigma-Aldrich) was added to the cells at 50 µg ml<sup>-1</sup> and the cells were incubated at 37 °C while being kept protected from light. The reaction was quenched by adding an excess of complete RPMI-10 media. Cells were then thoroughly washed three times by centrifugation at 300g for 10 min so as to remove all traces of mitomycin-c from the cells to reduce the potential of proliferative responses on the addition of the stimulator cells to the reaction. Cells were then resuspended in complete RPMI-10 and counted. Cells were plated at  $2-5 \times 10^5$  stimulator cells per well depending on the responder cell plating density. Stimulator cells were plated at a ratio of 1:3 (responder:stimulator). The plate was left to incubate for 7 days at 37 °C while kept protected from light. On day 7, the wells were stained with the following antibody panel: antihuman CD45-APC, CD3-PE, CD4-PerCP/Cy5.5, CD8-BUV395 and Violet LIVE/DEAD (BD Biosciences). Samples were then run on BD Influx FACS system and data were analyzed with FlowJo v.10 software.

CytoStim assay. CytoStim assays were performed following manufacturer's protocol (Miltenyi Biotec). In brief, spleen and bone marrow cells were collected from hu.Thor mice (12–18 weeks postoperation), and mixed at a 1:1 ratio in RPMI-1640 supplemented with 5% human AB serum at a density of  $1\times 10^7$  cells per ml.  $1.5\times 10^6$  cells were seeded in wells of round bottom 96-well plate, and treated with 3  $\mu$ l of CytoStim reagent. After 2 h of incubation at  $37\,^{\circ}\mathrm{C}$ , GolgiPlug (BD Biosciences) was added to the wells and the culture was continued for an additional 4 h. After incubation, cells were washed, fixed in cold BD Cytofix buffer for 20 min, followed by permeabilization with BD Perm/Wash buffer for 15 min. Cells were then pelleted and stained with the following human antibodies: CD45-BUV395, IL2-BV421, CD3-APC, IFN $\gamma$ -PE and TNF $\alpha$ -PerCP/Cy5.5, and analyzed with BD Influx FACS machine. Data were analyzed with FlowJo  $\nu$ -10 software. Immune cells collected from hu.PBMC mice (2–4 weeks postengraftment) were used as reference.

ELISpot analysis. The ELISpot assays were performed following the manufacturer's suggested protocol (Human IFN-γ ELISpot<sup>PLUS</sup> kit, MABTECH). Briefly, cells isolated from spleen and bone marrow of hu. Thor mice (12-18 weeks postoperation) were mixed at a 1:1 ratio and resuspended in RPMI medium containing 5% human AB serum. Cells of hu.PBMC mice (2-4 weeks postoperation), cryopreserved human PBMCs of healthy donors and nonhumnaized NSG mice were used as controls. Immune cells were seeded into 96-well stripes precoated with antihuman IFN-γ antibodies at 500,000 to 1 million cells per well (in duplicate or triplicate). The following stimulating agents were supplemented to each well: 3 µl human CytoStim (Miltenyi Biotec, 130-092-173),  $18.5\,\mu l$  of KLH (Sigma-Aldrich, 1003293900,  $5.4\,mg\,ml^{-1}$ ) and medium control. After 16 h of incubation at 37 °C, 5% CO<sub>2</sub>, the content in all the wells were decanted and the strips were washed with PBS five times in between detection antibody-biotin, streptavidin-ALP and substrate solution incubation. When distinct spots appeared on the membrane (10-30 min postincubation), chromogenic reaction was stopped by flushing the strips under running tap water in both sides. The membrane was dried overnight and subjected to imaging and spot counting with ImmunoSpot analyzer system (Cellular Technology Limited). The percentage and total number of hCD45+CD3+ T cells in each sample was obtained by FCM analysis. The number of IFN-γ producing cells in each sample was normalized to 10,000 CD3+ T cells.

Teratoma analysis. The CC1 iPS line (CW70296CC1) was purchased from Cellular Dynamics. The Y1 iPS line was established in house from skin fibroblast cells of healthy donors, and has been successfully induced to differentiate into (pro)insulin-producing pancreatic β cell-like cells, thymic epithelial progenitor cells and fibroblast-like cells. Both lines were maintained in mTeSR plus medium (StemCell Technology, 05825). Once confluent, cells were dissociated with ReLeSR (StemCell Technology, 05872) as aggregates. The collected cells were resuspended in culture medium at the concentration of  $1 \times 10^6$  per  $25 \,\mu$ l, mixed with equal volume of growth factor reduced Matrigel (Corning, 356231, thawed on ice), and were slowly drawn into an insulin syringe for intramuscular injection. Then  $1 \times 10^6$  iPSC aggregates were injected slowly to gastrocnemius muscle of anesthetized hu. Thor and hu. SRC recipients laying on their back, with CC1 cells on the left side and Y1 on the right side. 26 days after injections, the mice were euthanized for teratoma excision. All the tumor sizes are less than 2.0 cm at the largest diameter per Institutional Review Board policy at Allegheny Singer Research Institute. Excised teratomas were measured and weighed before proceeding to imaging analysis. Immunocompetent Friend virus B and immunocompromised NSG mice were used as negative and positive controls of teratoma formation, respectively.

Immunofluorescence and histological analysis. iPSC aggregates differentiated to TECs in polymerized alginate capsules were decapsulated by incubating with 100 mM EDTA for 2-3 min, which depolymerizes the alginate capsules enabling aggregate retrieval. The aggregates were then fixed with 4% PFA for 45 min at room temperature followed by washing in PBS (three times). The aggregates were labeled with primary antibodies for TEC markers. For mouse antihuman CD45 (Invitrogen MA5-17687, 1:200), mouse antihuman cytokeratin-8 (Cell Signaling Technologies, 4546S, 1:200), mouse antihuman CD205 (Biolegend), mouse antihuman DLL4 (Biolegend) and rabbit antihuman EpCAM (Cell Signaling Technologies) the aggregates were incubated with the primary antibodies diluted in PBS (1:50 unless specified otherwise) containing 10% donkey serum and were incubated overnight at 4 °C. The aggregates were washed with PBS (three times) before adding secondary antibodies diluted (1:500) in the same buffer: AlexaFluor donkey anti-Mouse 488 (Invitrogen) for the mouse primaries and AlexaFluor goat antirabbit 555 (Invitrogen) for rabbit primaries. The aggregates with secondary antibodies were incubated at 4°C overnight.

For labeling FOXN1, 3D iPSC-TECs were processed as above. Primary rabbit antihuman FoxN1 (Bioss) antibodies were diluted (1:50) in PBS containing 10% donkey serum and 1% Triton X-100 and were incubated overnight at 4°C followed by washing with PBS (three times) and then incubated with the appropriate secondaries diluted (1:500) in the same buffer as the primary antibodies overnight at 4°C. After the labeling process, the aggregates were washed with PBS (three times) before mounting onto a glass slide with Gold Antifade (Invitrogen) before imaging using Olympus Fluoview 2 confocal microscope. For FOXN1 labeling of human primary TECs (HTyEpiC, ScienCell Research Laboratories) and human primary lymphatic fibroblasts (ScienCell Research Laboratories), cells were recovered from frozen stock and cultured following the manufacturer's suggested protocol for 2-3 days. Cells were dissociated and fixed in 2.5% PFA solution/PBS at a concentration of  $2.5-5 \times 10^5$  cells per ml, and stored at 4 °C until Cytospin. To prepare the slides for immunofluorescence, the labeled colorfrost plus microscope slides were assembled (Fisherbrand), a cytofunnel (Epredia) added to the slide holder and these were placed in the centrifuge rack in the hood. Each funnel was filled with approximately ten drops of the fixed cell suspension. The spin was run under program 1 (12,000 r.p.m., 5 min) to obtain the slides with the cell containing spot ready for downstream staining (Thermo Scientific Cytospin Centrifuge). The same protocol was followed for FOXN1 labeling of the slides.

Teratoma tissue was collected for both immunofluorescence and hematoxin and eosin (H&E) histological analysis. Tissue being used for immunofluorescence staining was refrigerated in 4% PFA (Electron Microscopy Sciences) for 3 h, washed with PBS and placed in 30% sucrose solution at 4°C for at least 3 days. When ready for cutting, the tissue was briefly washed in PBS and embedded in Tissue Plus Optimal Cutting Temperature Clear embedding medium (Fisher HealthCare) over dry ice and cryosectioned into 8 µm sections using the Leica CM1950 cryostat (Leica). Once ready to stain, slides were removed from -20°C and rehydrated with PBS. Tissue was then fixed to the slide using 4% PFA, washed with PBS and permeabilized with 0.5% Triton X-100 (Sigma-Aldrich). Slides were washed again and blocked for 1 hour in 1% bovine serum albumin (Sigma-Aldrich) in PBS. After blocking, the tissue was washed, and the following primary antibodies (Abcam) were added at 1:100 dilution unless denoted and left to incubate overnight at 4°C: human anti-CD3 (Abcam ab11089) and anti-HLA-A (Abcam ab52922). Primary antibody was aspirated and tissue was washed in PBS before the following secondary antibodies (ThermoFisher) were added at 1:1,000 dilution for 1 h of incubation at room temperature: AlexaFluor 488 goat antirabbit IgG (A11034), AlexaFluor 555 goat antirat IgG (A21434), and AlexaFluor 594 donkey antimouse IgG (ab150108). Secondary antibody was aspirated and tissue was washed in PBS. Nuclei were then stained using ProLong Glass Antifade Mountant with NucBlue (Life Technologies Corporation). Slides were imaged using the Olympus Fluoview FV1000 confocal microscope (Olympus).

Teratoma tissue being used for H&E staining was collected and placed in 10% neutral buffered formalin (Richard-Allen Scientific). Tissue was then processed and stained within the Allegheny General Hospital Pathology department. Stained slides were then reviewed by multiple board-certified pathologists for appropriate interpretation and analysis.

Serum analysis to detect immunoglobulin class switching. Serum was harvested from hu. Thor mouse blood via either facial vein or cardiac puncture. Antibody Isotyping 7-Plex Human ProcartaPlex Panel (Invitrogen) was used to detect normal class-switching functions by testing for IgM, IgG, IgA and IgE levels within hu. Thor serum. The assay was run according to the manufacturer's protocol and was analyzed using the Luminex FLEXMAP 3D system (Luminex Corporation). Hu. Thor samples were compared to control untreated NSG mice to decrease the occurrence of false positives within the assay.

**Statistical analysis.** All values are expressed as the mean  $\pm$  standard deviation unless otherwise specified. Statistical analysis and comparisons were performed with GraphPad Prism v.8.0 using a two-tailed unpaired Student's t-test (GraphPad Software), unless specified otherwise. The following are the iterations used for P value significance: \*P < 0.05, \*\*P < 0.01, \*\*\*P < 0.001. All experiments were run at a minimum of n = 3 to gain statistical significance.

**Reporting summary.** Further information on research design is available in the Nature Research Reporting Summary linked to this article.

#### Data availability

All the data and materials are available from corresponding authors on reasonable request. Single-cell datasets (2D iPSC-TECs and 3D iPSC-TECs) are deposited at the National Centre for Biotechology Information Gene Expression Omnibus repository with accession number GSE201675. Source data are provided with this paper.

#### Code availability

The software code used to analyze scRNA-seq data is modified from the Seurat package (https://satijalab.org/seurat/), and is included in the supplementary information.

#### References

- Richardson, T. et al. in Programmed Morphogenesis: Methods and Protocols Methods in Molecular Biology (eds Ebrahimkhani, M. R. & Hislo, J.) 73–92 (Springer, 2021).
- Blondel, V. D., Guillaume, J.-L., Lambiotte, R. & Lefebvre, E. Fast unfolding of communities in large networks. *J. Stat. Mech.* 2008, P10008 (2008).

#### Acknowledgements

We thank E. Moravcikova for support with FCM, A. Sanguino for assistance with pathological assessment of teratomas, D. Graziano for assistance with HLA typing, H. Monroe and the University of Pittsburgh Genomics Research core for their expertise in scRNA preparation and analysis, and B. Phillips and W. Rudert for insightful suggestions and discussions of the project. Figure 3a was created with

BioRender.com. This study was supported in part by the National Institutes of Health (grant nos. Y.F., R01 AI123392 and R21 AI126335), National Science Foundation (Y.F. and I.B., CBET, standard grant no. 1804728), PA Health Department research grant (M.T., SAP no. 4100079708). C.M. and H.G. were supported by Highmark Health Award (grant no. A023948-HIGHMARK-LANNI-FAN). We also thank the Center for Biologic imaging University of Pittsburgh for the use of imaging facilities under the grant no. 1S10OD019973-01.

#### **Author contributions**

Y.F. and I.B. initiated the project. Y.F., I.B., M.T. and A.Z. designed the study. A.Z., C.W., W.L., C.M., A.T., H.C., H.G., R.K., S.W., S.B., R.L., R.K., L.B., B.M. and Y.F. performed experiments. A.A., C.M., Y.F. and Z.B.J. performed the computational analysis of scRNA-seq data. Y.F., A.Z. and I.B. wrote the manuscript. All authors reviewed and edited the manuscript.

#### **Competing interests**

The authors declare no competing interests.

#### Additional information

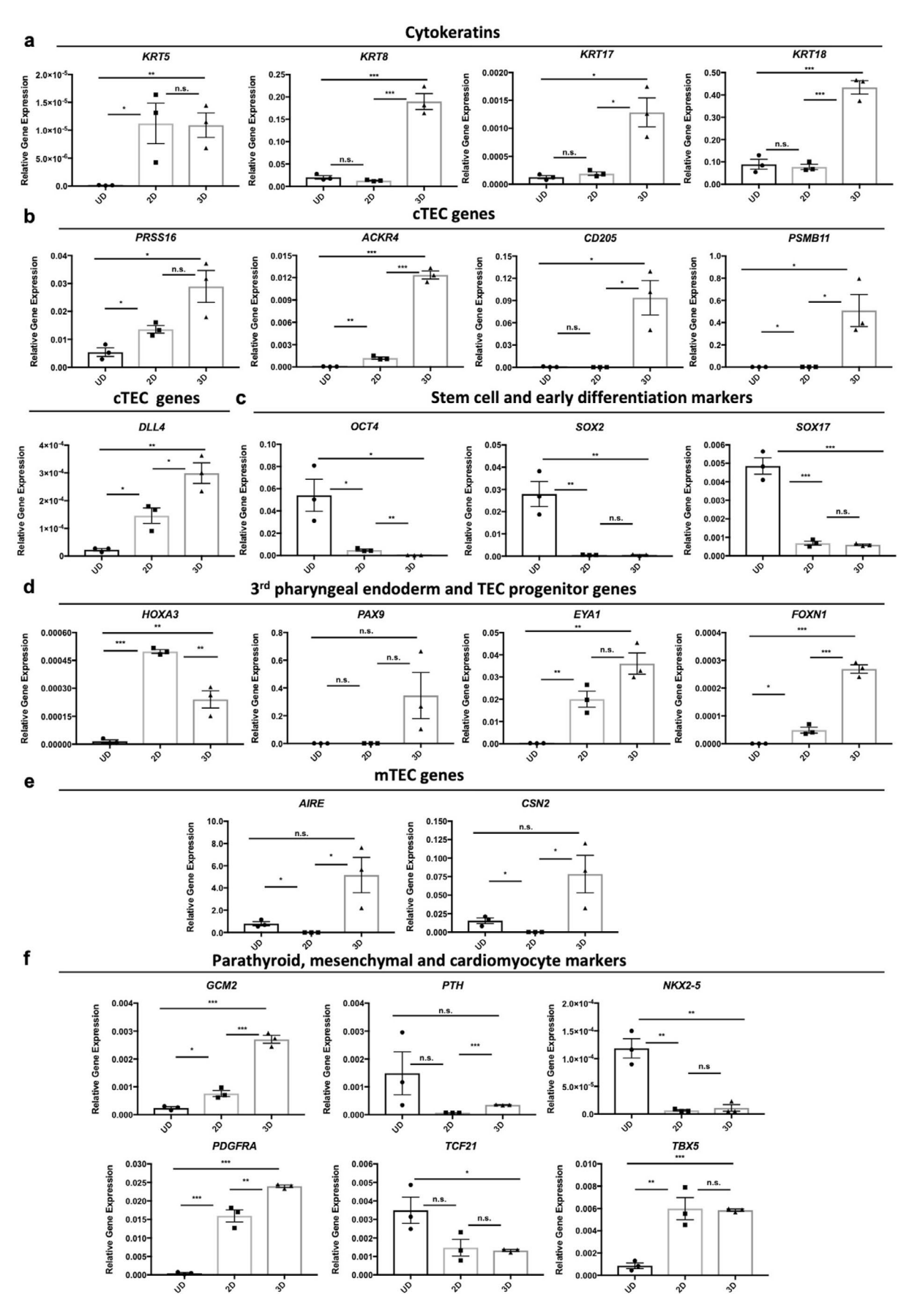
Extended data are available for this paper at https://doi.org/10.1038/s41592-022-01583-3.

**Supplementary information** The online version contains supplementary material available at https://doi.org/10.1038/s41592-022-01583-3.

Correspondence and requests for materials should be addressed to Yong Fan.

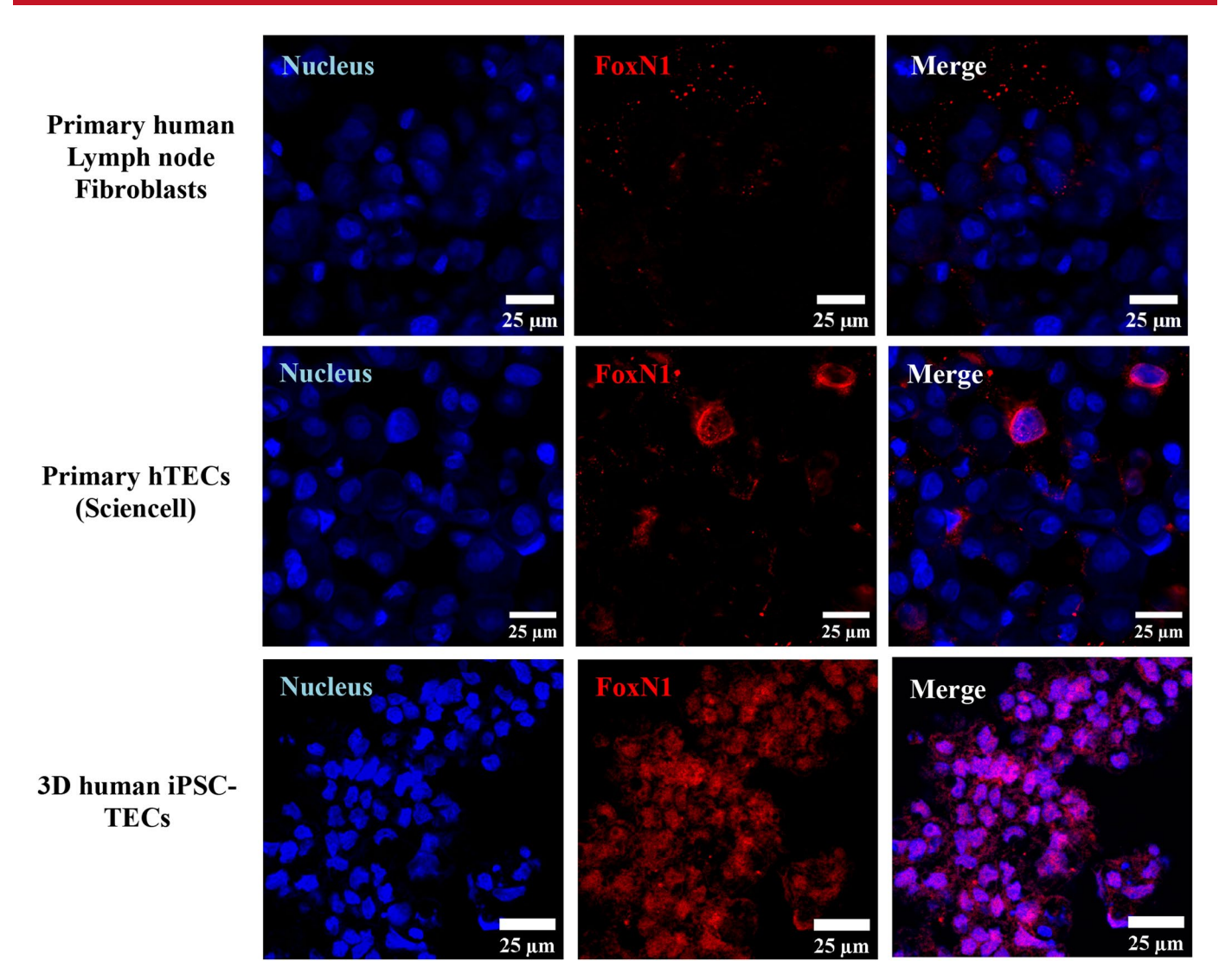
**Peer review information** *Nature Methods* thanks the anonymous reviewers for their contribution to the peer review of this work. Primary Handling Editor: Madhura Mukhopadhyay, in collaboration with the *Nature Methods* team.

Reprints and permissions information is available at www.nature.com/reprints.

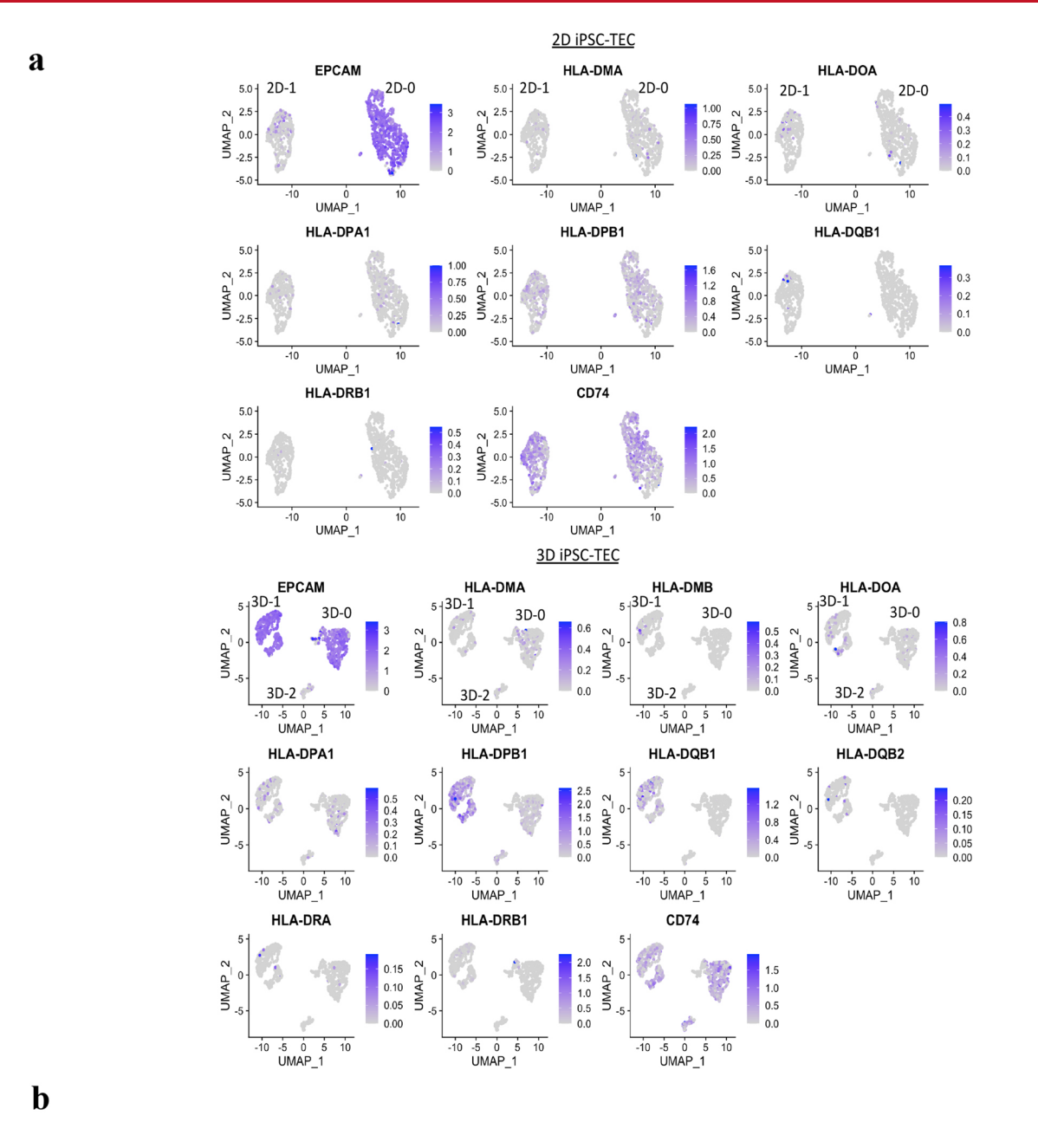


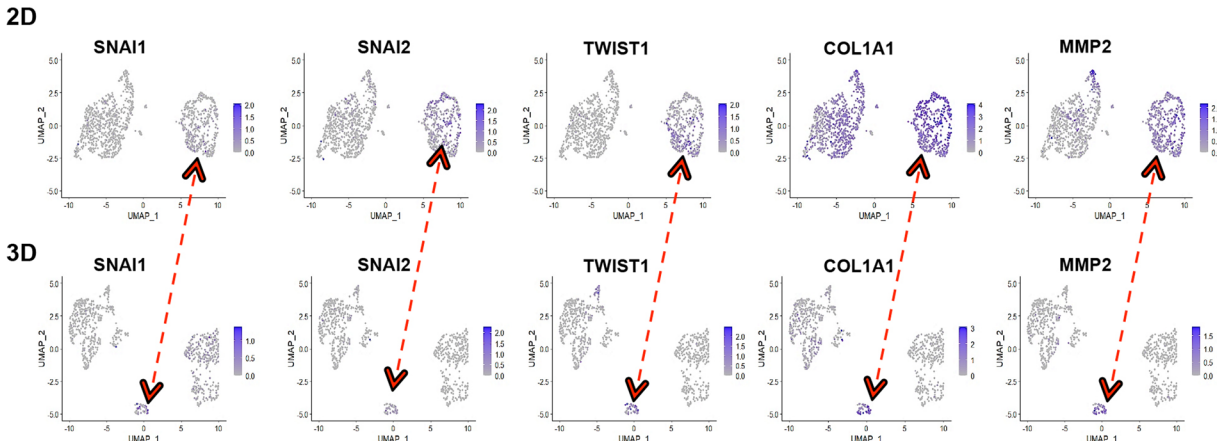
Extended Data Fig. 1 | See next page for caption.

**Extended Data Fig. 1 | RT-qPCR analysis of genes associated with TEC differentiation.** RNA samples were isolated from undifferentiated iPSCs (UD), 2D TECs (2D), and 3D TECs and were subjected to RT-qPCR analysis of expression of epithelium-associated cytokeratin genes (**a**), cortical TEC (cTEC)-specific genes (**b**), undifferentiated and early stem cell markers (**c**), early progenitors of the thymic epithelium (**d**), mTEC specific markers (**e**), and markers of the parathyroid (GCM and PTH), mesenchymal (TCF21 and PDGFRA), and cardiomyocyte lineages (NKX2-5 and TBX5) (**f**). Levels of gene expression were normalized to hGAPDH. Shown are results of triplicates from at least three independent isolations. Data are presented as mean values +/- SEM using a two-tailed unpaired t test. \* p < 0.05; \*\*\* p < 0.01; \*\*\*\* p < 0.005. Exact p values are listed in the Supporting Information.

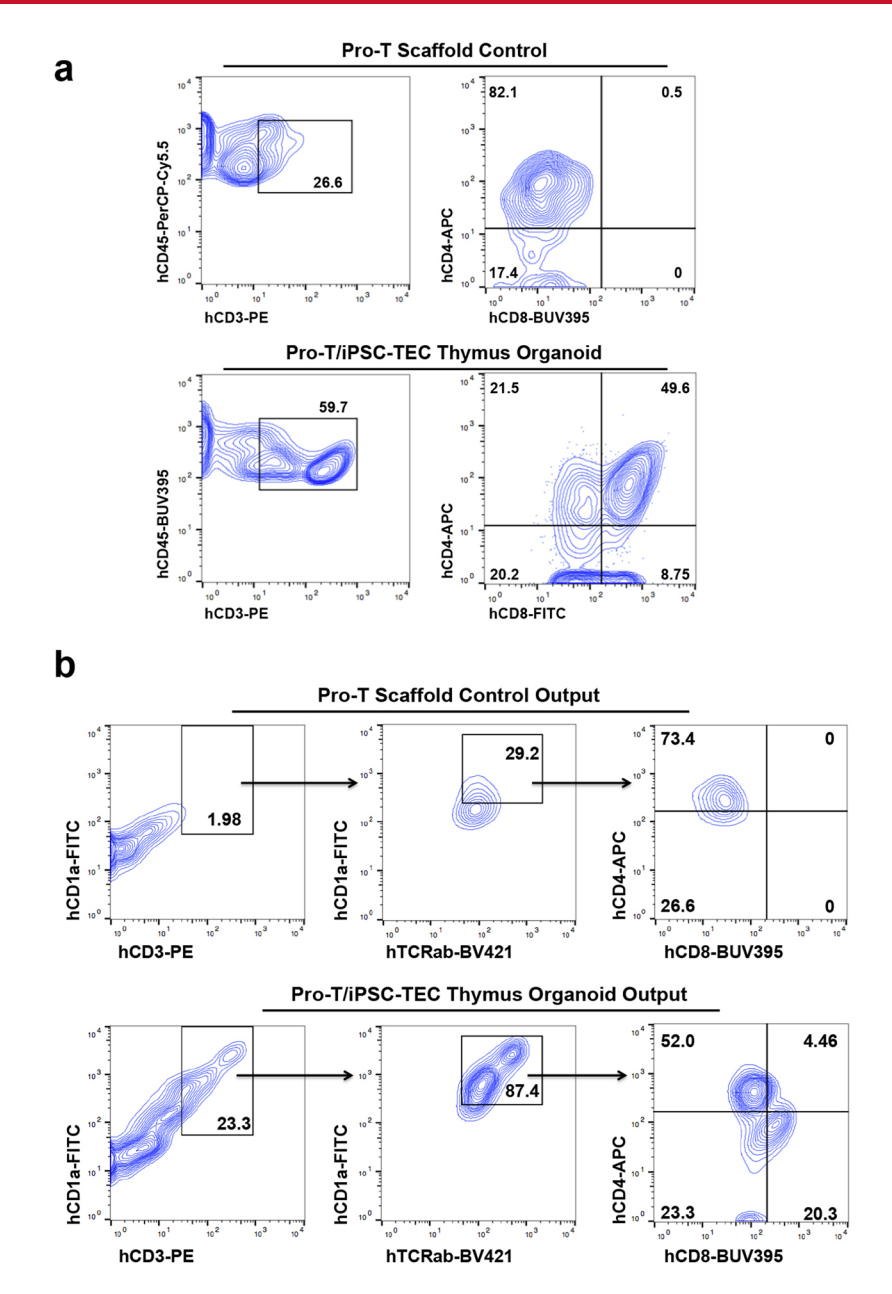


**Extended Data Fig. 2 | Immunofluorescence analysis of human FOXN1 expression in 3D iPSC-TECs.** Immunofluorescent images of 3D iPSC-TEC aggregates stained with antibodies against human FOXN1 (red) and counterstained with Hoechst 33342 for nucleus (blue). Primary human thymic epithelial cells and lymph node fibroblasts were used as positive and negative controls, respectively. White scale bar, 25um. Shown are representative images from three independent iPSC-TEC differentiations with similar results.

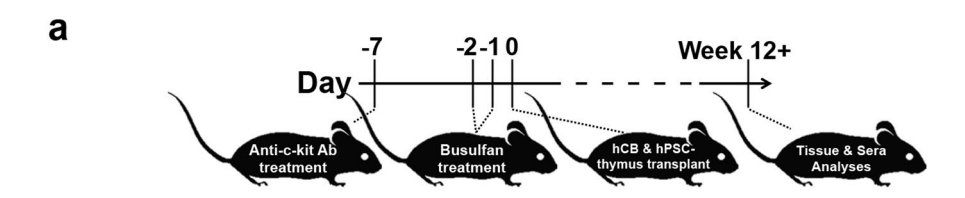




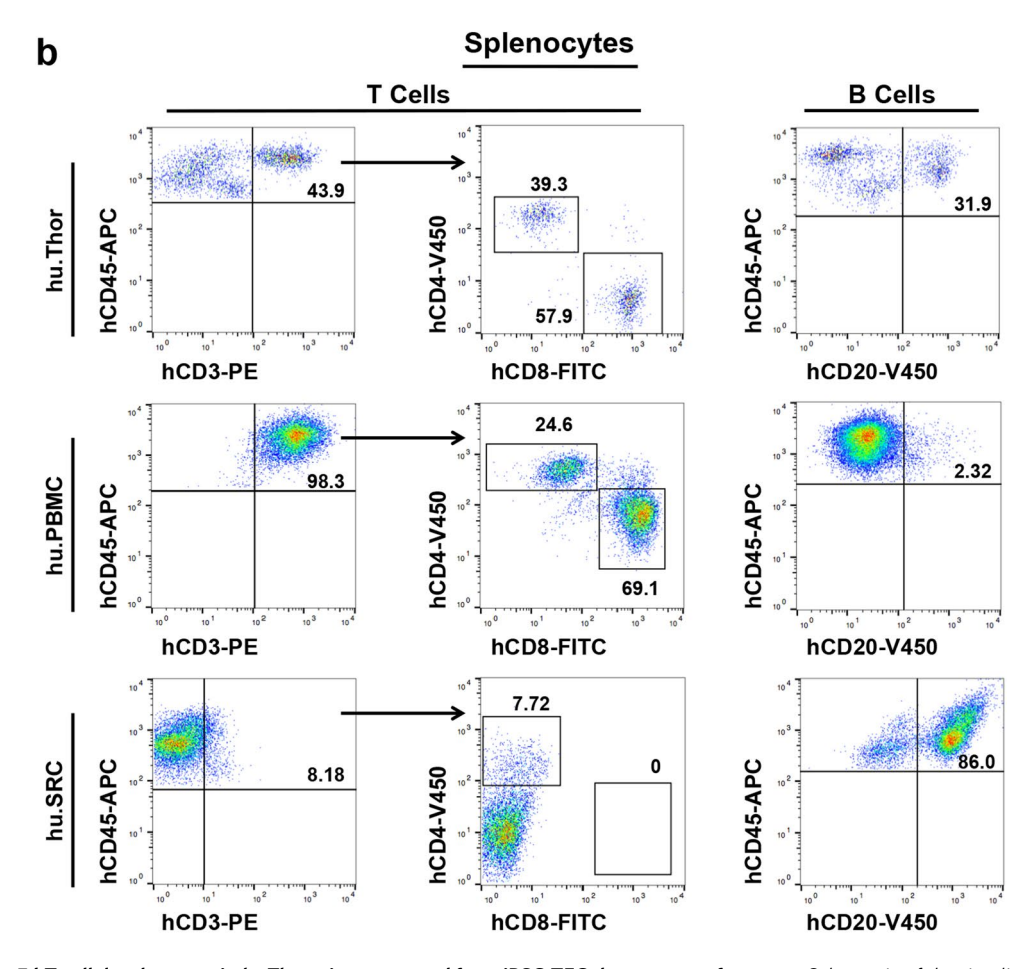
**Extended Data Fig. 3** | scRNA-seq analysis of iPSC-TECs. a. Annotation of key human leukocyte antigen (HLA) gene expression on 2D and 3D iPSC-TEC Seurat clusters. 3D iPSC-TECs display higher levels of HLA gene expression compared with 2D iPSC-TECs. b. c. Annotation of EMT-associated gene expression in 2D and 3D iPSC-TEC clusters, highlighting the phenotypic similarity between 2D-1 and 3D-2 clusters (double arrows).



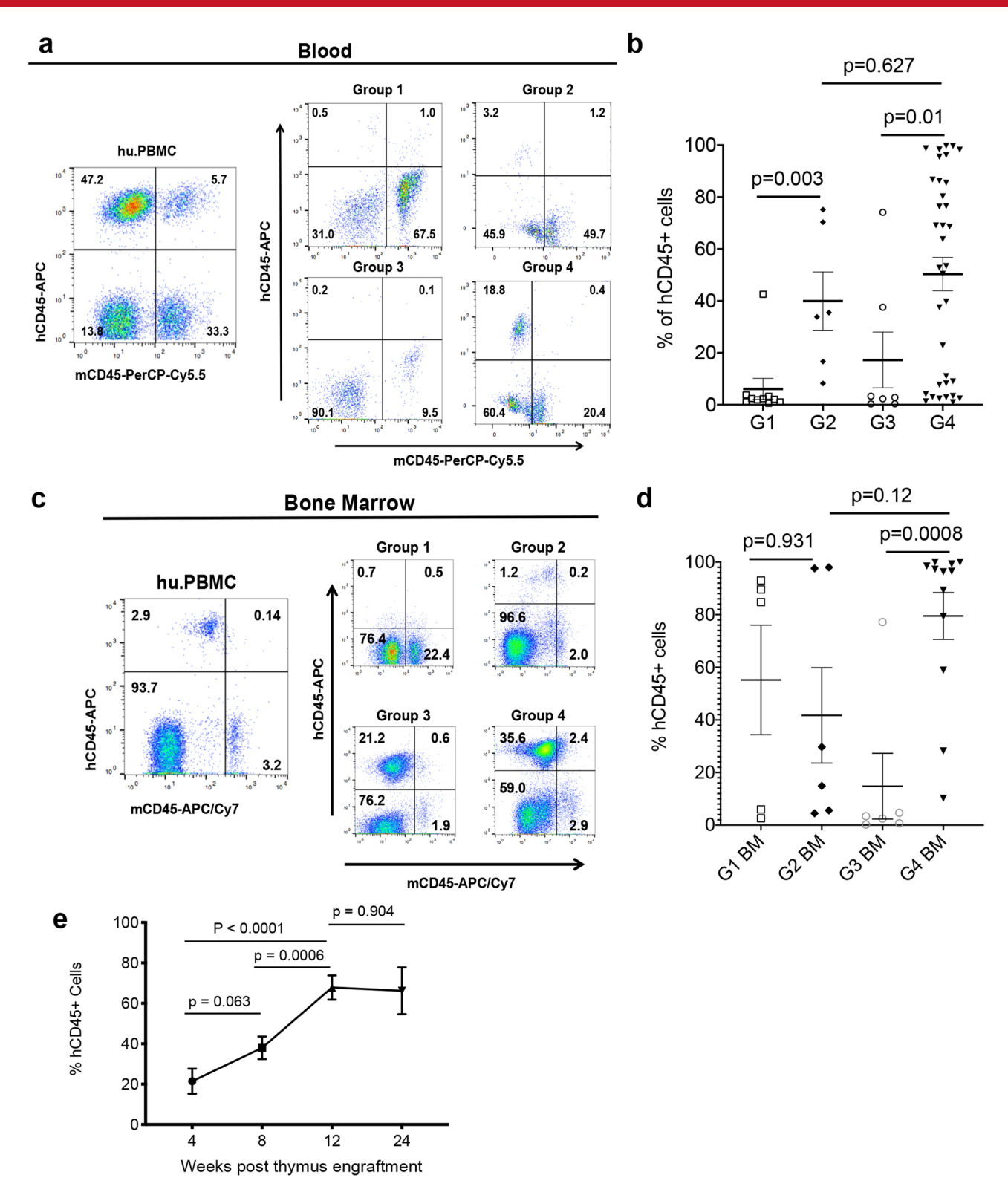
**Extended Data Fig. 4 | Pro-T/iPSC-TEC thymus organoids support progression of T cell development** *in vitro.* **a.** FCM analysis of CD4 and CD8 expression in cells of Pro-T/iPSC-TEC thymus organoids (*lower panels*) after one week of *in vitro* culture. *Upper panels*, cells dissociated from one week cultured decellularized scaffolds seeded with Pro-T cells alone (Pro-T scaffolds) as controls. Shown are representative FCM graphs from at least three independent experiments with similar results. **b.** FCM analysis of thymic output from Pro-T/iPSC-TEC thymus organoids (*lower panels*) and Pro-T scaffold controls (*upper panels*). hCD45+ cells were examined for key surface markers of T cell development (CD1a+CD3+, *left columns*), TCRab (*middle columns*), and CD4 and CD8 (*right columns*). Shown are representative graphs of at least two independent experiments for the Pro-T control output and at least five independent experiments for Pro-T/iPSC-TEC thymus organoid output with similar results.



|            | Humaniz       | ed Mouse | Group Genera   | ition                |
|------------|---------------|----------|----------------|----------------------|
|            | Anti-c-kit Ab | Busulfan | hCB Transplant | Thymus<br>Transplant |
| Group<br>1 |               | ~        | ~              |                      |
| Group<br>2 |               | V        | ~              | V                    |
| Group<br>3 | V             | V        | ~              |                      |
| Group<br>4 | ~             | ~        | ~              | V                    |

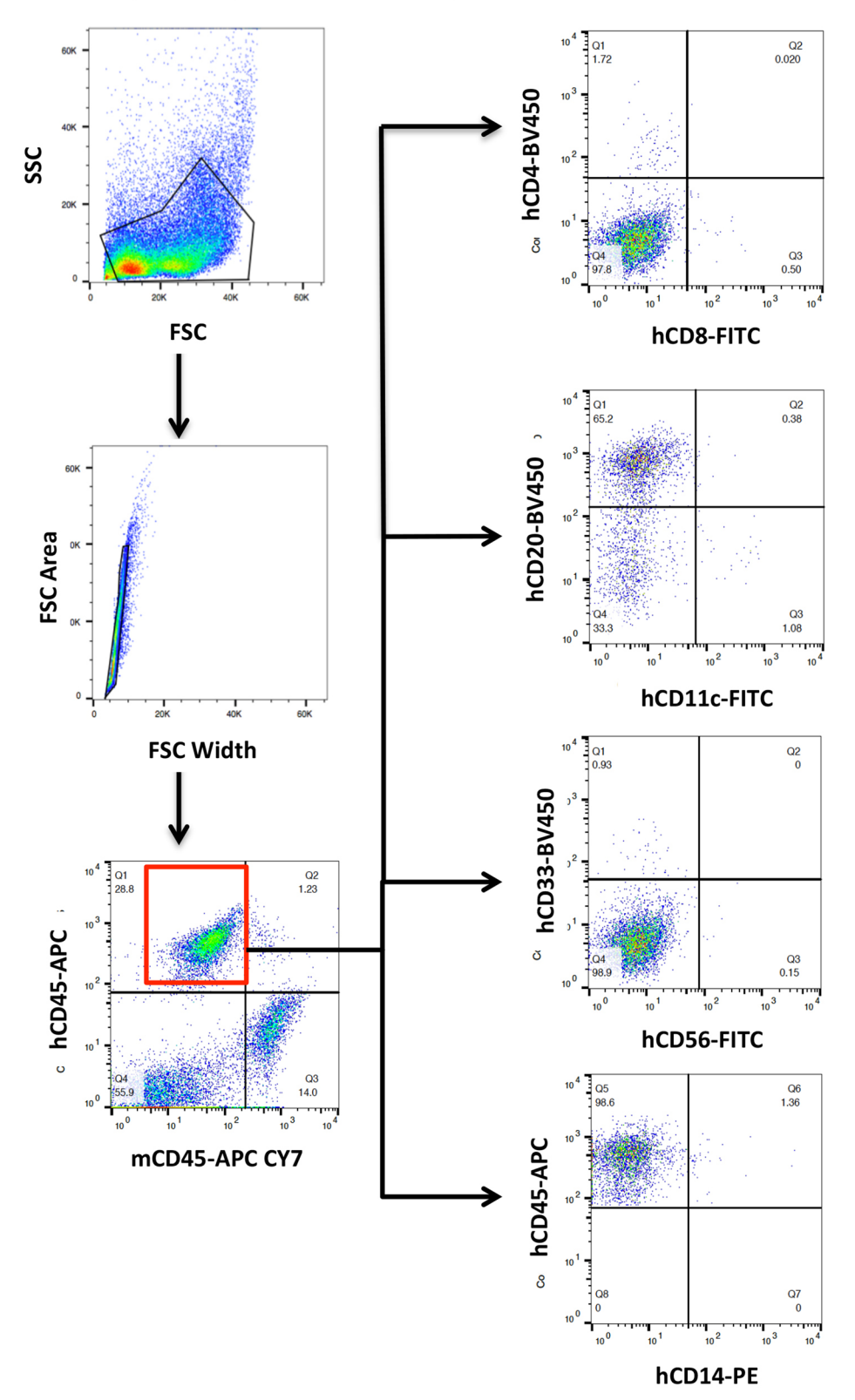


**Extended Data Fig. 5 | T cell development in** *hu.Thor* **mice generated from iPSC-TEC thymus engraftment. a.** Schematic of the timeline (*upper panel*) and treatments (*lower panel*) of four groups (G1-G4) of humanized mice. **b.** FCM analysis of hCD4+ and hCD8+T cells (*middle panels*) in the hCD45+mCD45-hCD3+ gate (*left panels*) and CD20+B cells (*right panels*) of *hu.Thor, hu.PBMC*, and *hu.SRC* mice. Shown are representative FCM graphs from at least four mice of each type with similar results.

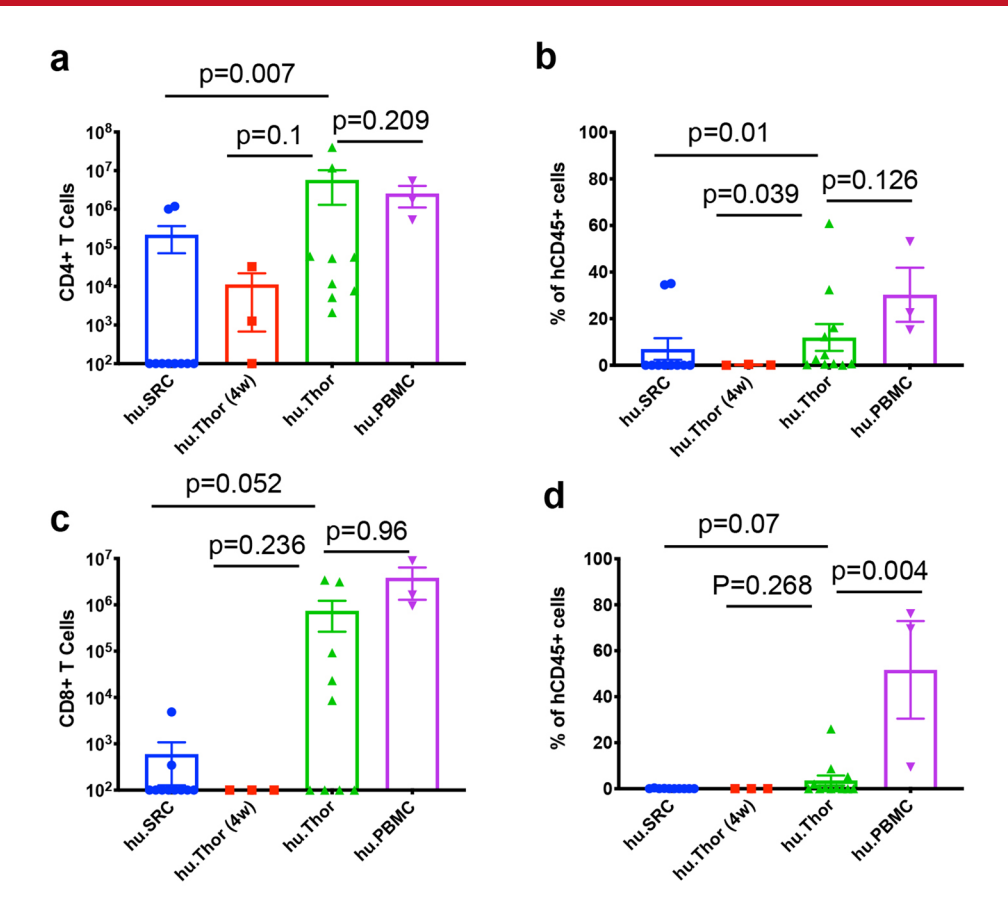


**Extended Data Fig. 6 | HPC/iPSC-TEC thymus-engrafted** *hu* mice displayed increased human cell chimerisim over time. **a.** FCM analysis of human CD45+(hCD45+) versus mouse CD45+(mCD45+) cells in peripheral blood of G1-G4 mice at 12-weeks post-transplantation. Left panel shows hu.PBMC blood as a positive control. Shown are representative graphs from at least five independent mice from each group with similar results. **b.** Dot plots showing percentages of hCD45+ cells in peripheral blood of four groups of *hu* mice (G1-G4) at 12-week post-transplantation. Data are shown as mean +/- SEM, analyzed by two-tailed, Mann-Whitney test. **c-d.** Cells were isolated from the bone marrow of G1-G4 *hu* mice (18-40 weeks post-transplantation) and analyzed with FCM for overall ratios of human cell chimerism (% of hCD45 in total CD45+cells). **c.** Representative FCM graphs from at least five independent mice from each group. **d.** Dot plots showing the percentages of hCD45+ cells as mean +/- SEM, analyzed by two-tailed, Mann-Whitney test. **e.** Progression of hCD45+ cell chimerism in *hu.Thor* mice with time. Shown are % of hCD45+ cells (over total CD45+cells) in peripheral blood of hu.Thor mice 4 (n=9), 8 (n=28), 12 (n=25) and 24 (n=10) weeks post iPSC-TEC thymus transplantation. Data are denoted as mean +/- SEM with two-tailed, unpaired Welch's t test.

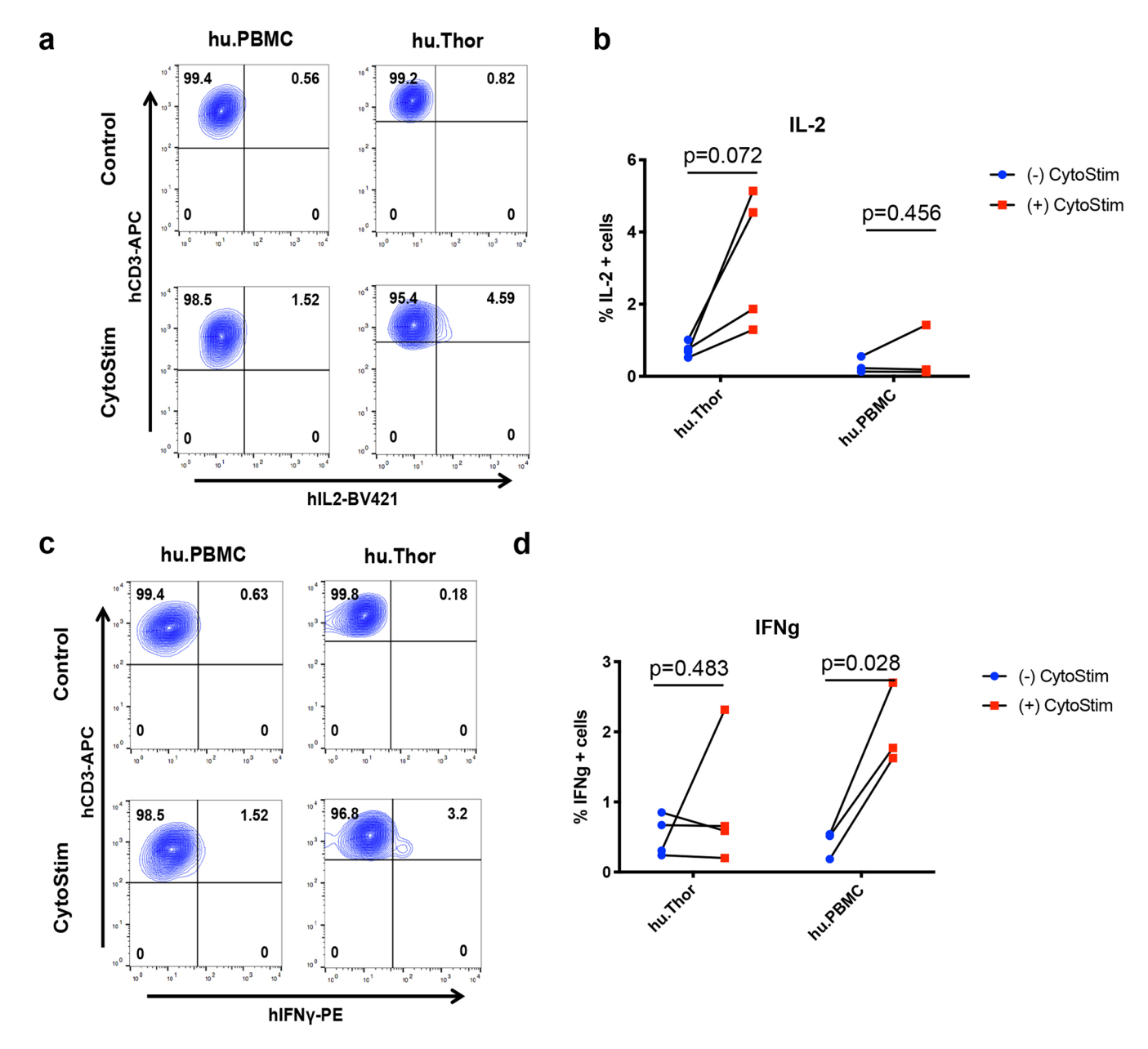
# Gating Strategies for analyzing human immune cell subsets



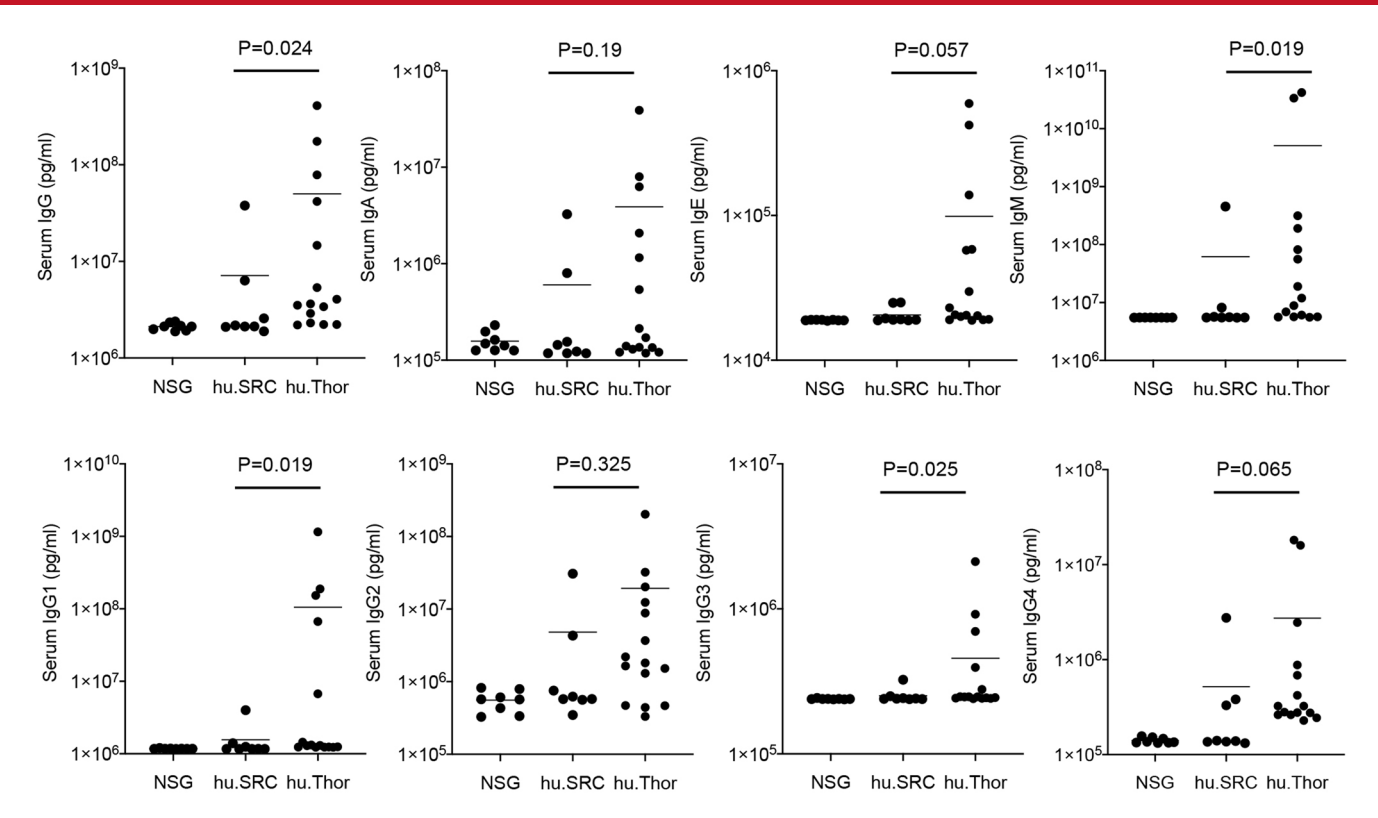
**Extended Data Fig. 7 | Multiple hematopoietic lineage development in** *hu.Thor* mice after 4-weeks of iPSC-TEC thymus transplantation. Gating strategy for characterization of *hu.Thor* splenocytes. Singlets were then gated on hCD45 versus mCD45, and only hCD45+ cells were used as the entry gate into lineage study. Staining was completed for T cells (CD4 and CD8, top right panel), B cells and dendritic cells (CD20 and CD11c, second from top right panel), myeloid and NK cells (CD33 and CD56, third from the top right panel), and monocyte cells (CD14, bottom panel). Shown are representative of three independent experiments with similar results.



**Extended Data Fig. 8 | Generation of CD4+ and CD8+T cells in** hu. Thor mice. Splenocytes were harvested from hu. SRC (n=10), hu. Thor at 4 weeks post-transplantation (4w), hu. Thor (n=9, 16-weeks) and hu. PBMC mice and analyzed with FCM for CD4+ and CD8+T cell populations. **a** and **c**. Total numbers of CD4+T cells (**a**) and CD8+T cells (**c**). **b** and **d**. Percentage of CD4+T cells (**b**) and CD8+T cells (**d**). Data are presented as bar graphs with mean values +/- SEM using a two-tailed Mann-Whitney test, where p < 0.05 is considered as significance.



**Extended Data Fig. 9 | CytoStim-mediated IL-2 and IFNg production in** hu.Thor **CD3+T-cells.** Splenocytes and bone marrow cells were harvested and mixed at 1:1 ratio from hu.Thor (n = 4) and hu.PBMC (n = 3), and stimulated with CytoStim (**a** and **c**, lower panels) for 6 hours, and intracellularly stained for IL-2 (**a** and **b**) and IFNg (**c** and **d**). **a** and **c**. FCM analysis of IL2- (**a**) and IFNg- (**c**) producing cells in the hCD45+CD3+T cell populations. Shown are representative FCM graphs from three independent experiments with similar results. **b** and **d**. Percentages of IL2+ (**b**) and IFNg+ (**d**) hCD3+T cells before (blue dots) and after (red dots) CytoStim stimulation. Data were analyzed with paired, two-tailed t-test. p < 0.05 is considered as significance.



**Extended Data Fig. 10** | Generation of major human immunoglobulin classes in hu.Thor mice. Sera were harvested from hu.Thor mice (n=15) at 16-18 weeks post-transplantation. Isotypes of human immunoglobulin classes were quantified with Luminex isotyping kit. Upper rows show the primary classes of immunoglobulin. Lower rows show the lgG subclasses. Sera from hu.SRC mice (n=8) at similar post-transplant ages were used as controls. Sera from untreated NSG mice (n=8) were used as negative control to show the background of the assay. Data are shown as dot plots with mean (bar). Statistical analysis was performed between hu.SRC and hu.Thor samples with a two-tailed Mann-Whitney test. p < 0.05 is considered as significance.

# nature research

| Corresponding author(s):   | Yong Fan   |
|----------------------------|------------|
| Last updated by author(s): | 05/12/2022 |

# **Reporting Summary**

Nature Research wishes to improve the reproducibility of the work that we publish. This form provides structure for consistency and transparency in reporting. For further information on Nature Research policies, see our <u>Editorial Policies</u> and the <u>Editorial Policy Checklist</u>.

For all statistical analyses, confirm that the following items are present in the figure legend, table legend, main text, or Methods section.

| <u> </u>   |     |    |     |     |        |
|------------|-----|----|-----|-----|--------|
| <b>C</b> 1 | - ~ | +1 | ist | 11. | $\sim$ |
| . วา       |     |    | וכו | -11 |        |

| n/a         | Confirmed  |
|-------------|--|
|             | $oxed{\boxtimes}$ The exact sample size (n) for each experimental group/condition, given as a discrete number and unit of measurement  |
|             | 🔀 A statement on whether measurements were taken from distinct samples or whether the same sample was measured repeatedly  |
|             | The statistical test(s) used AND whether they are one- or two-sided  Only common tests should be described solely by name; describe more complex techniques in the Methods section.  |
| $\boxtimes$ | A description of all covariates tested   |
| $\times$    | A description of any assumptions or corrections, such as tests of normality and adjustment for multiple comparisons  |
|             | A full description of the statistical parameters including central tendency (e.g. means) or other basic estimates (e.g. regression coefficient) AND variation (e.g. standard deviation) or associated estimates of uncertainty (e.g. confidence intervals) |
|             | For null hypothesis testing, the test statistic (e.g. <i>F</i> , <i>t</i> , <i>r</i> ) with confidence intervals, effect sizes, degrees of freedom and <i>P</i> value noted <i>Give P values as exact values whenever suitable.</i>                        |
| $\boxtimes$ | For Bayesian analysis, information on the choice of priors and Markov chain Monte Carlo settings   |
| $\boxtimes$ | For hierarchical and complex designs, identification of the appropriate level for tests and full reporting of outcomes   |
| $\boxtimes$ | Estimates of effect sizes (e.g. Cohen's <i>d</i> , Pearson's <i>r</i> ), indicating how they were calculated   |
|             | Our web collection on <u>statistics for biologists</u> contains articles on many of the points above.  |

#### Software and code

Policy information about availability of computer code

Data collection

Odyssey infrared scanner (LI-COR Biosciences), BD FACS Influx (v.1.2.0.142, BD Biosciences), LightCycler 480II (v.1.5, Roche), Nanodrop Spectrophotometer (Nanodrop), Bioanalyzer 2100 (Agilent), nCounter Max Gen 2 (Nanostring Technologies), Olympus FV10ASW (v.03.01.03.03, Olympus), Luminex xPonent for FLEXMAP 3D (v.4.2 Build 1513, Luminex Corporation), 10X Genomics Chromium Controller (10X Genomics), ImmunoSpot (S6 Micro, Cellular Technology Limited)

Data analysis

FlowJo (v.10.7.1, Becton Dickinson & Company), GraphPad Prism (v.7.0e and v.8, GraphPad Software), Microsoft Excel for Mac 2011 (v.14.7.7, Microsoft), ImageJ (v.1.50i, NIH), Fiji (v.1.53c, NIH), Seurat R Package (v.4.0.1), nSolver 4.0 Advanced (Nanostring Technologies), Cell Ranger (v5 and v6, 10X Genomics), ImmunoCapture (v.6.5)

For manuscripts utilizing custom algorithms or software that are central to the research but not yet described in published literature, software must be made available to editors and reviewers. We strongly encourage code deposition in a community repository (e.g. GitHub). See the Nature Research guidelines for submitting code & software for further information.

#### Data

Policy information about availability of data

All manuscripts must include a data availability statement. This statement should provide the following information, where applicable:

- Accession codes, unique identifiers, or web links for publicly available datasets
- A list of figures that have associated raw data
- A description of any restrictions on data availability

All the data are available from the corresponding author on reasonable request. The scRNA datasets were uploaded to GEO, and the The GEO accession number is GSE201675. Figures associated with raw data include Figs 1, 3, 4 and 5.

|      |   | 1    |          | • • | •   |    |        | 100 | •    |
|------|---|------|----------|-----|-----|----|--------|-----|------|
| Fiel |   | 1-51 | )e       | CIT | IC  | re | no     | rti | ıng  |
|      | _ | י י  | <u> </u> | 011 | . • |    | $\sim$ |     | '''' |

| i lelu-spe                  | cinc reporting   |  |  |  |  |
|-----------------------------|--|--|--|--|--|
| Please select the o         | ne below that is the best fit for your research. If you are not sure, read the appropriate sections before making your selection.  |  |  |  |  |
| ∑ Life sciences             | Behavioural & social sciences Ecological, evolutionary & environmental sciences  |  |  |  |  |
| For a reference copy of     | the document with all sections, see <u>nature.com/documents/nr-reporting-summary-flat.pdf</u>  |  |  |  |  |
|                             |  |  |  |  |  |
| Lifo scior                  | ocas study dasign  |  |  |  |  |
| Life Sciel                  | nces study design  |  |  |  |  |
| All studies must dis        | sclose on these points even when the disclosure is negative.   |  |  |  |  |
| Sample size                 | No statistical methods were used to predetermine sample size. At least 3 samples were used for each group for statistical analysis. Due to the large variation of long-term HSC composition in CD34+ progenitor cells from each cord blood isolation, and the long duration time from transplantation to detectable human cell chimerism, it is difficult to predetermine the number of mice needed. Statistical tools are used to analyze the samples to examine significance.  |  |  |  |  |
| Data exclusions             | Humanized mice displaying less than 0.5% of hCD45+ cells in their peripheral blood at 12 weeks post-human cells engraftment or at the time of sacrifice were excluded from the study.  |  |  |  |  |
| Replication                 | Multiple human pluripotent stem cell lines (one hESC line, and 3 human iPSC lines) were examined in the in vitro study, and two lines were used in the in vivo study. Similar results were observed in all the lines tested. All experiments, whether they included cells or not, were replicated at least 3 times both biologically and technically, that is, with a minimum of 3 different biological samples, run a minimum of 3 different times on the appropriate machinery or under the same assay conditions. This replication does not include our scRNA analysis, where we were only able to submit one sample of each type to be analyzed in a high throughput manner. Our submitted data reflect the success of the replications, where the heterogeneity of our samples is reflected in some variation, but the integrity of our findings is shown in the data's significance.   |  |  |  |  |
| Randomization               | Age and gender matched NSG mice (both males and females) were randomly alloted to receive thymus+HSC or HSC alone.   |  |  |  |  |
| Blinding                    | Lymphocytic infiltration of teratomas was evaluated by pathologists in blind fashion. All the flow cytometry data were acquired by dedicated operators in blind fashion. Data collection and initial data analysis were also performed blind.  |  |  |  |  |
| We require informati        | g for specific materials, systems and methods on from authors about some types of materials, experimental systems and methods used in many studies. Here, indicate whether each material, ted is relevant to your study. If you are not sure if a list item applies to your research, read the appropriate section before selecting a response.  |  |  |  |  |
|                             | perimental systems Methods   |  |  |  |  |
| n/a Involved in th          |  |  |  |  |  |
| Antibodies                  | ChIP-seq   |  |  |  |  |
| Eukaryotic                  | cell lines   |  |  |  |  |
| Palaeonto                   | ogy and archaeology MRI-based neuroimaging   |  |  |  |  |
| Animals and other organisms |  |  |  |  |  |
|                             | earch participants   |  |  |  |  |
| Clinical dat                |  |  |  |  |  |
| Dual use re                 | esearch of concern   |  |  |  |  |
| Antibodies                  |  |  |  |  |  |
| Antibodies used             | Based on staining of 0.5 to 1 million cells in 100uL  • Mouse anti-CD45-APC-Cy7 (clone 30-F11) BD Biosciences Cat #557659 (2ul/test)  • Human anti-CD45-APC (clone HI30) BD Biosciences Cat #555485 (2ul/test)  • Human anti-CD3-PE (clone HIT3a) BD Biosciences Cat #555340 (5ul/test)  • Human anti-CD4-V450 (clone RPA-T4) BD Biosciences Cat #560345 (5ul/test)  • Human anti-CD8-FITC (clone HIT8a) BD Biosciences Cat #555634 (5ul/test)  • Human anti-CD20-V450 (clone L27) BD Biosciences Cat #561164 (5ul/test)  • Human anti-CD11c-FITC (clone B-ly6) BD Biosciences Cat #561355 (5ul/test)  • Human anti-CD14-PE (clone MφP9) BD Biosciences Cat #562691 (5ul/test)  • Human anti-CD56-FITC (clone B159) BD Biosciences Cat #562794 (5ul/test)  • Human anti-CD45RO-FITC (clone UCHL1) BD Biosciences Cat #555492 (5ul/test)  • Human anti-CD45RA-PE (clone HI100) BD Biosciences Cat #555489 (5ul/test)  • Human anti-FoxP3-PE (clone PCH101) eBioscience Cat #12-4776-42 (2ul/test) |  |  |  |  |

- Human anti-CD25-V450 (clone M-A251) BD Biosciences Cat #560355 (5ul/test)
- Human anti-CCR6-BV421 (clone 11A9) BD Biosciences Cat #562515 (5ul/test)
- Human anti-CXCR3-BV510 (clone 1C6/CXCR3) BD Biosciences Cat #740183 (5ul/test)
- Human anti-MHC Class II-PerCP-Cy5.5 (clone G46-6) BD Biosciences Cat #552764 (2ul/test)
- Human anti-EpCAM-PE (clone 1B7) eBioscience Cat #12-9326-42 (2ul/test)
- Human anti-TCRβ-PE (clone T10B9.1A-31) BD Biosciences Cat #561674 (5ul/test)
- Human anti-TCRγδ-FITC (clone B1) BD Biosciences Cat #559878 (5ul/test)
- Human anti-CD4-FITC (clone RPA-T4) BD Biosciences Cat #555346 (5ul/test)
- Human anti-CD8-PerCP-Cy5.5 (clone RPA-T8) BD Biosciences Cat #560662 (5ul/test)
- Human anti-CD5-APC (clone UCHT2) Biolegend Cat # 300612 (4ul/test)
- Human anti-CD7-PerCP-Cy5.5 (clone CD7-6B7) Biolegend Cat #343116 (4ul/test)
- Human anti-CD4-APC (clone L200) BD Biosciences Cat #551980 (4ul/test)
- Human anti-CD8-BUV395 (clone RPA-T8) BD Biosciences Cat #563795 (5ul/test)
- Human anti-CD45-PerCP-Cy5.5 (clone HI30) BD Biosciences Cat #564105 (2ul/test)
- Human anti-CD1a-BV421 (clone HI149) BD Biosciences Cat #563938 (5ul/test)
- Human anti-EpCAM-BV421 (clone EBA-1) BD Biosciences Cat #563180 (2ul/test)
- Human anti-DLL4-PE (clone MHD4-46) Biolegend Cat #346505 (5ul/test)
- Human anti-CD205-BV510 (clone MMRI-7) BD Biosciences Cat #744057 (5ul/test)
- Mouse anti-CD45-APC (clone 30-F11) BD Biosciences Cat #559864 (2ul/test)
- Mouse anti-CD45-PerCP-Cy5.5 (clone 30-F11) BD Biosciences Cat #550994 (2ul/test)
- Human anti-CD45-BUV395 (clone HI30) BD Biosciences Cat #563792 (5ul/test)
- Human anti-CD3-APC (clone OKT3) Biolegend Cat #317318 (5ul/test)
- Human anti-IL-2-BV421 (clone MQ1-17H12) Biolegend Cat #500327 (5ul/test)
- Human anti-TNFα-PerCP-Cy5.5 (clone MAb11) Biolegend Cat #502925 (5ul/test)
- Human anti-IFNy-FITC (clone B27) Biolegend Cat #506506 (5ul/test)
- Th1/Th17 Phenotyping Kit BD Biosciences Cat #560759 (20ul of cocktail/test)
- Anti-CD4-PerCP-Cy5.5 (clone RM4-5)
- Anti-IL-17A-PE (clone TC11-18H10.1)
- Anti-IFNy-FITC (clone XMG1.2)
- BV421 Mouse IgG1 Isotype Control (clone X40) BD Biosciences Cat #562438 (5ul/test)
- APC Mouse IgG1 Isotype Control (clone MOPC-21) BD Biosciences Cat #555751 (5ul/test)
- FITC Mouse IgG1 Isotype Control (clone MOPC-21) BD Biosciences Cat #555748 (5ul/test)
- APC-Cy7 Rat IgG2b Isotype Control (clone A95-1) BD Biosciences Cat #552773 (5ul/test)
- V450 Mouse IgG1 Isotype Control (clone MOPC21) BD Biosciences Cat #560373 (5ul/test)
- PE Rat IgG1 Isotype Control (clone R3-34) BD Biosciences Cat #553925 (5ul/test)
- BV510 Rat IgG2b Isotype Control (clone R35-38) BD Biosciences Cat #562951 (5ul/test)
- PerCP-Cy5.5 Mouse IgG1 Isotype Control (clone MOPC-21) BD Biosciences Cat #550795 (5ul/test)
- APC Rat IgG2a Isotype Control (clone eBR2a) eBioscience Cat #17-4321-81 (5ul/test)
- FITC Hamster IgG1 Isotype Control (clone A19-3) BD Biosciences Cat #553971 (5ul/test)
- PerCP-Cy5.5 Rat IgG2a Isotype Control (clone R35-95) BD Biosciences Cat #550765 (5ul/test)

#### Immunofluorescence:

- Human anti-CD3-unconjugated Abcam Cat #ab11089 (dilution 1:100)
- Human anti-HLA-A-unconjugated Abcam Cat #ab52922 (dilution 1:100)
- Human anti-CD45-unconjugated Invitrogen Cat #MA5-17687 (dilution 1:500)
- Human anti-keratin 8/18-unconjugated Cell Signaling Technologies Cat #4546S (dilution 1:200)
- Human anti-EpCAM-unconjugated Cell Signaling Technologies Cat #36746S (dilution 1:50)
- Human anti-CD205-unconjugated Biolegend Cat # 359202 (dilution 1:50)
- Human anti-DLL4-unconjugated Biolegend Cat # 346502 (dilution 1:50)
- Human anti-keratin 14-unconjugated R&D Systems Cat #
- Human anti-FoxN1-unconjugated Bioss Cat # BS6970R (dilution 1:50)
- Goat anti-rabbit IgG AlexaFluor 488 ThermoFisher Cat #A11034 (dilution 1:1000)
- Goat anti-rat IgG AlexaFluor 555 ThermoFisher Cat #A21434 (dilution 1:1000)
- Donkey anti-mouse IgG AlexaFluor 594 Abcam Cat #ab150108
- Donkey anti-mouse IgG AlexaFluor 488 ThermoFisher Cat #A-21202

Validation

All the antibodies used in the studies were obtained from reliable vendors/manufacturers, including BD biosciences, Biolegends, and ThermoFisher, which have programs to perform vigorous validation for their antibodies. All the antibodies used in the study came with manufacturer's validation statement in the data sheets.

# Eukaryotic cell lines

Policy information about cell lines

Cell line source(s)

H1 hESC line (WiCell Research Institute), CC1 (CW70296CC1), and EE1 (CW70028EE1) were purchased from Cellular Dynamics (Fuji Films). Fibroblastic lymph node cells were purchased from SciencCell Research Laboratories. The Y1 iPS line was generated and tested in house.

Authentication

Pluripotency of all the cell lines used in the study was tested by teratoma formation analysis and stem cell marker expression, as well as morphological identification and growth properties. In addition, both H1 and Y1 lines were induced to differentiated into proinsulin-producing pancreatic beta cell like cells. All cell lines were induced to differentiated into thymic epithelial progenitor cells, as shown in this study.

Mycoplasma contamination

All cell lines tested negative for mycoplasma in house.

## Animals and other organisms

Policy information about studies involving animals; ARRIVE guidelines recommended for reporting animal research

Laboratory animals

8-12 week old male and female NSG mice (Jackson Laboratory) were used to construct hematopoietic humanized mice. 3-4 week old male and female CD1 (Charles River) were used for thymus scaffold preparation. 12-16 week old male and female FVB mice (Jackson Laboratory) were used as controls in the teratoma assay. Mice are housed in optimal environmental conditions, including a 14-hour light/10-hour dark cycle, 65-75oF temperature and 40-60% humidity.

Wild animals

No wild animals were used in this study.

Field-collected samples

No field-collected samples were used in this study.

Ethics oversight

All animal procedures were approved by the Allegheny General Hospital Institutional Animal Care and Use Committee, and in adherence to the NIH Guide for the Care and Use of Laboratory Animals.

Note that full information on the approval of the study protocol must also be provided in the manuscript.

## Flow Cytometry

#### **Plots**

Confirm that:

- The axis labels state the marker and fluorochrome used (e.g. CD4-FITC).
- 💢 The axis scales are clearly visible. Include numbers along axes only for bottom left plot of group (a 'group' is an analysis of identical markers).
- All plots are contour plots with outliers or pseudocolor plots.
- A numerical value for number of cells or percentage (with statistics) is provided.

#### Methodology

Sample preparation

A detailed description of all sample preparations for FACS analysis can be found in the Methods section. For hu.Thor tissue staining, spleen, bone marrow, and blood samples were collected from mice. Blood was diluted with PBS and put on a Ficoll gradient to remove RBC and then stained for the desired markers. Splenocytes and bone marrow cells were isolated and put through RBC lysis before being pelleted and counted for eventual staining.

For TEC staining, 3D capsules were dissolved and cells were placed on a Ficoll gradient to remove any debris and dead cells prior to staining. 2D TECs were trypsinized from the plate and washed in PBE prior to staining. Scaffolds were enzymatically digested and put on a Ficoll gradient to remove dead cells prior to being stained.

Instrument

BD FACS Influx (v.1.2.0.142, BD Biosciences) was used for all the FCM data presented, except Supplemental Fig. S12 (right panels), which were collect on MACSQuant Analyzer with the MACSQuantify Software (version 2, Miltenyi Biotec).

Software

BD Influx sorting software for data acquisition and Flowjo (version 10.7) for analysis.

Cell population abundance

No cell populations were sorted by flow cytometry.

Gating strategy

Ficoll separated live cells were defined by FSC/SSC and LIVE/DEAD Fixable dead cell stain kit (ThermoFisher). Singlets were gated on FSC-A/FSC-W. Further gating strategies can be found in Supplemental Figure S10.

| Tick this box to confirm that a figure exemplifying the gating strategy is provided in the Supplementary Information.